ARMY RESEARCH LABORATORY

Analysis of Shock Compression of Strong Single Crystals With Logarithmic Thermoelastic-Plastic Theory

by John D. Clayton

ARL-RP-481 **May 2014**

A reprint from the *International Journal of Engineering Science*, Vol. 79, pp. 1–20, 2014.

NOTICES

Disclaimers

The findings in this report are not to be construed as an official Department of the Army position unless so designated by other authorized documents.

Citation of manufacturer's or trade names does not constitute an official endorsement or approval of the use thereof.

Destroy this report when it is no longer needed. Do not return it to the originator.

Army Research Laboratory
Aberdeen Proving Ground, MD 21005-5069

ARL-RP-481 **May 2014**

Analysis of Shock Compression of Strong Single Crystals With Logarithmic Thermoelastic-Plastic Theory

John D. Clayton
Weapons and Materials Research Directorate, ARL

A reprint from the *International Journal of Engineering Science*, Vol. 79, pp. 1–20, 2014.

REPORT DOCUMENTATION PAGE

Form Approved
OMB No. 0704-0188

1. REPORT DATE *(DD-MM-YYYY)*	**2. REPORT TYPE**	**3. DATES COVERED (From - To)**
May 2014	Reprint	May 2013–May 2014

4. TITLE AND SUBTITLE
Analysis of Shock Compression of Strong Single Crystals With Logarithmic Thermoelastic-Plastic Theory

5a. CONTRACT NUMBER

5b. GRANT NUMBER

5c. PROGRAM ELEMENT NUMBER

6. AUTHOR(S)
John D. Clayton

5d. PROJECT NUMBER
DRI13-WMR-019

5e. TASK NUMBER

5f. WORK UNIT NUMBER

7. PERFORMING ORGANIZATION NAME(S) AND ADDRESS(ES)
U.S. Army Research Laboratory
ATTN: RDRL-WMP-C
Aberdeen Proving Ground, MD 21005-5069

8. PERFORMING ORGANIZATION REPORT NUMBER
ARL-RP-481

9. SPONSORING/MONITORING AGENCY NAME(S) AND ADDRESS(ES)

10. SPONSOR/MONITOR'S ACRONYM(S)

11. SPONSOR/MONITOR'S REPORT NUMBER(S)

12. DISTRIBUTION/AVAILABILITY STATEMENT
Approved for public release; distribution is unlimited.

13. SUPPLEMENTARY NOTES
A reprint from the *International Journal of Engineering Science*, Vol. 79, pp. 1–20, 2014.

14. ABSTRACT
A finite strain theory is developed for anisotropic single crystals undergoing shock loading. Inelastic deformation may arise from dislocation slip, twinning, or fracture and crack sliding. Internal energy can generally depend on a logarithmic measure of finite elastic strain, entropy, and an internal variable associated with defect accumulation. A closed form analytical solution is derived for the planar shock response in the thermoelastic regime, at axial stresses up to the Hugoniot elastic limit. In the plastic regime, for highly symmetric orientations and rate independent shear strength, the Rankine–Hugoniot conditions and constitutive relations can be reduced to a set of algebraic equations that can be solved for the material response. The theory is applied towards planar shock loading of single crystals of sapphire, diamond, and quartz. Logarithmic elasticity is demonstrated to be more accurate (i.e., requires fewer higher-order elastic constants) than Lagrangian or Eulerian theories for sapphire, diamond, and Z-cut quartz. Results provide new insight into criteria for initiation of twinning, slip, and/or fracture in these materials as well as their strength degradation when shocked at increasingly higher pressures above the Hugoniot elastic limit.

15. SUBJECT TERMS
shock physics, elasticity, plasticity, finite strain, crystals

16. SECURITY CLASSIFICATION OF:			**17. LIMITATION OF ABSTRACT**	**18. NUMBER OF PAGES**	**19a. NAME OF RESPONSIBLE PERSON**
a. REPORT	**b. ABSTRACT**	**c. THIS PAGE**			John D. Clayton
Unclassified	Unclassified	Unclassified	UU	26	**19b. TELEPHONE NUMBER** (*Include area code*) 410-278-6146

International Journal of Engineering Science 79 (2014) 1–20

Contents lists available at ScienceDirect

International Journal of Engineering Science

journal homepage: www.elsevier.com/locate/ijengsci

Analysis of shock compression of strong single crystals with logarithmic thermoelastic-plastic theory

J.D. Clayton *

Impact Physics, RDRL-WMP-C, US Army Research Laboratory, Aberdeen Proving Ground, MD 21005-5066, USA

ARTICLE INFO

Article history:
Received 14 November 2013
Received in revised form 10 February 2014
Accepted 13 February 2014

Keywords:
Shock physics
Elasticity
Plasticity
Finite strain
Crystals

ABSTRACT

A finite strain theory is developed for anisotropic single crystals undergoing shock loading. Inelastic deformation may arise from dislocation slip, twinning, or fracture and crack sliding. Internal energy can generally depend on a logarithmic measure of finite elastic strain, entropy, and an internal variable associated with defect accumulation. A closed form analytical solution is derived for the planar shock response in the thermoelastic regime, at axial stresses up to the Hugoniot elastic limit. In the plastic regime, for highly symmetric orientations and rate independent shear strength, the Rankine–Hugoniot conditions and constitutive relations can be reduced to a set of algebraic equations that can be solved for the material response. The theory is applied towards planar shock loading of single crystals of sapphire, diamond, and quartz. Logarithmic elasticity is demonstrated to be more accurate (i.e., require fewer higher-order elastic constants) than Lagrangian or Eulerian theories for sapphire, diamond, and Z-cut quartz. Results provide new insight into criteria for initiation of twinning, slip, and/or fracture in these materials as well as their strength degradation when shocked at increasingly higher pressures above the Hugoniot elastic limit.

Published by Elsevier Ltd.

1. Introduction

The response of solids to shock compression under planar impact has been a subject of intensive study over the past half-century (McQueen, Marsh, Taylor, Fritz, & Carter, 1970), including numerous advances in experiments, theoretical/analytical methods, and numerical techniques. Regarding modeling of related phenomena, much effort has centered on development of the pressure–volume equation-of-state (EOS) applicable for loading regimes or materials (e.g., very high pressures, or isotropic fluids and ductile solids) wherein shear strength and anisotropy are of little or no concern. However, for strong solids–ceramics, minerals, and some metals and alloys, for example – significant shear strength is retained under impact loading at moderate to high pressures. This strength can affect the global response of the material in loading conditions pertinent to ballistic penetration, geologic events, explosions, high-speed vehicular collisions, etc. Microstructure, including grain or constituent orientation and presence of multiple phases, can also significantly affect the shock response (Grady, 1984). In shocked single crystals of high purity which are the focus of the present work, crystal lattice orientation is the primary descriptor of initial microstructure, and it affects anisotropic themoelasticity and orientation-dependent inelasticity (e.g., slip, twinning, and cleavage fracture).

* Tel.: +1 410 278 6146; fax: +1 410 278 2460.
E-mail address: john.d.clayton1.civ@mail.mil

http://dx.doi.org/10.1016/j.ijengsci.2014.02.016
0020-7225/Published by Elsevier Ltd.

In Section 2 of this paper, a new finite deformation, anisotropic thermoelastic theory is developed for single crystals, and is applied to study the shock response of oriented crystals of sapphire (α-Al_2O_3), diamond (C), and quartz (α-SiO_2). These materials are considered because (i) they exhibit a high Hugoniot Elastic Limit (HEL), enabling assessment of finite strain effects in their elastic shock response and (ii) ample data on higher-order elastic constants (Graham, 1972; Hankey & Schuele, 1970; Nielsen, 1986; Thurston, McSkimin, & Andreatch, 1966) and planar shock compression experiments (Graham & Brooks, 1971; Fowles, 1967; Lang & Gupta, 2010) exist, enabling model development and validation.

In recent prior work (Clayton, 2013), a finite strain theory based on strain measure $\boldsymbol{D} = \frac{1}{2}(\boldsymbol{1} - \boldsymbol{F}^{-1}\boldsymbol{F}^{-\mathrm{T}})$ was developed and compared to usual nonlinear crystal thermoelasticity (Clayton, 2011a; Thurston, 1974; Wallace, 1972) based on the Green strain $\boldsymbol{E} = \frac{1}{2}(\boldsymbol{F}^{\mathrm{T}}\boldsymbol{F} - \boldsymbol{1})$, where $\boldsymbol{F}$ is the deformation gradient. These are respectively referred to as "Eulerian" and "Lagrangian" theories (Nielsen, 1986; Thomsen, 1972), though both strain measures are referred to material coordinates and are thus admissible in thermodynamic potentials for anisotropic solids [in contrast to the Almansi strain $\boldsymbol{A} = \frac{1}{2}(\boldsymbol{1} - \boldsymbol{F}^{-\mathrm{T}}\boldsymbol{F}^{-1})$, for example, used in isotropic nonlinear elasticity]. Eulerian theory demonstrated advantages with regards to describing the compression and shear reponses of ideal cubic crystals with Cauchy symmetry, and demonstrated greater intrinsic stability (Clayton & Bliss, 2014) than Lagrangian theory for these conditions. Analytical solutions to the planar shock problem were also derived using both models, with predictions compared for sapphire, diamond, and quartz (Clayton, 2013). Neither model was definitively superior for describing the shock response of these real anisotropic single crystals, with elastic constants of up to order three or four necessary in either case. Anisotropic Lagrangian-type nonlinear elastic models of crystals have been used by other authors in numerical simulations of wave propagation (Winey & Gupta, 2004) and spall (Foulk & Vogler, 2010). Recently, the aforementioned Eulerian theory has been applied towards new nonlinear elastic solutions of boundary value problems involving discrete lattice defects (Clayton, in press).

In the novel thermoelastic theory developed in the current work, internal energy is a function of entropy and material logarithmic strain $\boldsymbol{e} = \ln \boldsymbol{U}$, where $\boldsymbol{U}$ is the right stretch in the polar decomposition $\boldsymbol{F} = \boldsymbol{RU} = \boldsymbol{VR}$, with $\boldsymbol{R}$ the rotation. Elastic theory based on Hencky's strain measure $\ln \boldsymbol{V}$ has been used to accurately model isotropic solids at moderate-to-large strains (Anand, 1979), but this Eulerian theory does not apply for anisotropic solids. Regarding the latter, hyperelastic theory based on $\boldsymbol{e}$ has been considered with regards to derivation of higher-order elastic constants in cubic crystals (Dlużewski, 2000), but such theory has remained, until now, untested for stress states involving both pressure and shear such as uniaxial strain shock compression. Success of the logarithmic pressure–volume EOS, to which $\boldsymbol{e}$-based theory degenerates under hydrostatic loading, has been demonstrated (Poirier & Tarantola, 1998). In Section 2.1, a complete thermodynamically consistent nonlinear thermoelasticity theory incorporating $\boldsymbol{e}$ is derived and presented for the first time. A new analytical solution to the planar shock problem for solids obeying this constitutive theory is derived in Section 2.2. Application of the solution to sapphire, diamond, and quartz follows in Section 2.3, wherein advantages of the proposed logarithmic formulation over existing Lagrangian and Eulerian thermoelasticity models become clear.

Recently (Srinivasa, 2012), a promising structure for anisotropic hyperelasticity has been developed that involves decomposition of $\boldsymbol{F}$ into the product of an orthogonal matrix and an upper triangular matrix, with strain energy depending on the latter. This approach, though not explored in the current paper, demonstrates certain advantages regarding computational efficiency and physical interpretation relative to models that use a polar decomposition (e.g., logarithmic theory).

In Section 3, the logarithmic theory is extended to address inelastic deformation, wherein the deformation gradient is split into thermoelastic ($\boldsymbol{F}^{\mathrm{E}}$) and inelastic ($\boldsymbol{F}^{\mathrm{P}}$) parts: $\boldsymbol{F} = \boldsymbol{F}^{\mathrm{E}}\boldsymbol{F}^{\mathrm{P}}$ (Clayton, 2011a; Teodosiu & Sidoroff, 1976), implying existence of a stress free intermediate or natural configuration (Rajagopal & Srinivasa, 1998) from which the material exhibits an instantaneous thermoelastic response. Typical crystal plasticity models of high rate behavior have used the elastic Green strain measure $\boldsymbol{E} = \frac{1}{2}(\boldsymbol{F}^{\mathrm{ET}}\boldsymbol{F}^{\mathrm{E}} - \boldsymbol{1})$ in their nonlinear elastic stress–strain relations (Clayton, 2005a, 2005b; Luscher, Bronkhorst, Alleman, & Addessio, 2013; Vogler & Clayton, 2008; Winey & Gupta, 2006). In Section 3.1 of the current work, logarithmic thermoelastic strain $\boldsymbol{e} = \ln \boldsymbol{U}^{\mathrm{E}}$ is used as a state variable in the internal energy, where $\boldsymbol{F}^{\mathrm{E}} = \boldsymbol{R}^{\mathrm{E}}\boldsymbol{U}^{\mathrm{E}} = \boldsymbol{V}^{\mathrm{E}}\boldsymbol{R}^{\mathrm{E}}$. Inelastic deformation $\boldsymbol{F}^{\mathrm{P}}$ may result from a host of physical mechanisms in single crystals, including dislocation slip (Clayton, McDowell, & Bammann, 2004; Teodosiu & Sidoroff, 1976), deformation twinning (Clayton, 2009), pore collapse (Barton, Winter, & Reaugh, 2009; Clayton, 2008), and/or cleavage fracture on preferred planes (Aslan, Cordero, Gaubert, & Forest, 2011; Clayton, 2006). Thermodynamically consistent elastic–plastic models incorporating logarithmic strain measures have been developed elsewhere for isotropic solids (Xiao, Bruhns, & Meyers, 2007); several known previous logarithmic models for anisotropic elastic–plastic crystals (Barton et al., 2009; Clayton & Becker, 2012) have posited constitutive equations for deviatoric stress and pressure directly (the latter with an EOS), in a way not necessarily consistent with existence of a hyperelastic total energy potential.

Solution of the planar elastic–plastic shock problem is derived in Section 3.2, wherein a rate independent, but history dependent, deformation system-level shear strength model is applied in the context of the logarithmic theory. The Rankine–Hugoniot conditions (Germain & Lee, 1973) and constitutive relations yield a set of coupled nonlinear algebraic equations that can be solved iteratively for the themomechanical state downstream from a plastic shock, with the upstream state corresponding to the elastic precursor. The analysis extends a prior treatment of isotropic solids (Perrin & Delannoy-Coutris, 1983). Previous analytical solutions for elastic–plastic wave propagation in crystals have been restricted to small strain theory (linear elasticity) and isentropic conditions (Johnson, 1972, 1974; Johnson, Jones, & Michaels, 1970); the present work, in contrast, incorporates large deformation, nonlinear themoelasticity, and entropy production. In Section 3.3, model predictions are compared with experimental data on sapphire, diamond, and quartz shocked in pure mode directions above the

HEL, demonstrating accuracy of the model when proper inelastic deformation mechanisms are incorporated for each crystal type. Conclusions are given in Section 4, and the logarithmic pressure–volume EOS is discussed in the Appendix A.

Notation of continuum physics is used: vectors and tensors are bold, scalars and scalar components are italic, and summation holds for repeated subscripted indices (Cartesian coordinates). Superscripts T, −1, and −T denote the transpose, inverse, and inverse-transpose. Scalar and tensor products obey $\boldsymbol{a}\cdot\boldsymbol{b}=a_Kb_K$, $\boldsymbol{A}:\boldsymbol{B}=A_{IJ}B_{IJ}$, and $(\boldsymbol{a}\otimes\boldsymbol{b})_{IJ}=a_Ib_J$.

2. Anisotropic logarithmic thermoelasticity

2.1. Continuum theory

Spatial and referential coordinates are related by the motion $\boldsymbol{x}=\boldsymbol{x}(\boldsymbol{X},t)$. The deformation gradient $\boldsymbol{F}$ and its determinant are

$$\boldsymbol{F}=\nabla_0\boldsymbol{x}\quad(F_{iJ}=\partial_J x_i),\quad J=\det\boldsymbol{F}=\frac{\rho_0}{\rho}>0. \tag{2.1}$$

Initial and current mass densities are ρ_0 and ρ. Let $\boldsymbol{P}$ and $\boldsymbol{\sigma}$ denote first Piola–Kirchhoff and Cauchy stress:

$$\boldsymbol{P}=J\boldsymbol{\sigma}\boldsymbol{F}^{-\mathrm{T}};\quad P_{iJ}=J\sigma_{ik}F^{-1}_{Jk}=\frac{\rho_0}{\rho}\sigma_{ik}\partial_k X_J. \tag{2.2}$$

Let $\boldsymbol{v}=\dot{\boldsymbol{x}}$ be particle velocity, where the superposed dot is a material time derivative. Balances of linear and angular momentum in the absence of body force are

$$\nabla_0\cdot\boldsymbol{P}=\rho_0\dot{\boldsymbol{v}};\quad \partial_J P_{iJ}=\rho_0\ddot{x}_i; \tag{2.3}$$

$$\boldsymbol{P}\boldsymbol{F}^{\mathrm{T}}=\boldsymbol{F}\boldsymbol{P}^{\mathrm{T}};\quad P_{iJ}F_{kJ}=P_{kJ}F_{iJ}. \tag{2.4}$$

Let Ψ and U denote Helmoltz free energy and internal energy per unit initial volume, and let θ and η denote absolute temperature and entropy density; then

$$U=\Psi+\theta\eta. \tag{2.5}$$

For homogeneous thermoelastic solids, in general,

$$\Psi=\Psi\,(\boldsymbol{F},\theta),\quad U=U\,(\boldsymbol{F},\eta). \tag{2.6}$$

Dependence on $\boldsymbol{F}$ will be replaced later by dependence on a logarithmic strain measure that respects rotational invariance of the thermodynamic potentials.

The local balance of energy, in the absence of scalar heat sources, is

$$\dot{U}=\boldsymbol{P}:\dot{\boldsymbol{F}}-\nabla_0\cdot\boldsymbol{Q};\quad \dot{U}=P_{iJ}\partial_J\dot{x}_i-\partial_J Q_J; \tag{2.7}$$

with $\boldsymbol{Q}$ heat flux in reference coordinates. Local entropy production obeys

$$\dot{\eta}+\nabla_0\cdot(\boldsymbol{Q}/\theta)\geqslant 0;\quad \theta\dot{\eta}+\partial_J Q_J-(Q_J\partial_J\theta)/\theta\geqslant 0. \tag{2.8}$$

Using (2.5) and (2.7) in (2.8),

$$\boldsymbol{P}:\dot{\boldsymbol{F}}-\eta\dot{\theta}-\dot{\Psi}-(\boldsymbol{Q}\cdot\nabla_0\theta)/\theta\geqslant 0. \tag{2.9}$$

Then from the first of (2.6),

$$(\boldsymbol{P}-\partial\Psi/\partial\boldsymbol{F}):\dot{\boldsymbol{F}}-(\eta+\partial\Psi/\partial\theta)\dot{\theta}-\boldsymbol{Q}\cdot\nabla_0\theta\geqslant 0, \tag{2.10}$$

from which the standard thermoelastic constitutive equations of hyperelasticity follow:

$$\boldsymbol{P}=\partial\Psi/\partial\boldsymbol{F},\quad \eta=-\partial\Psi/\partial\theta. \tag{2.11}$$

From (2.5) and (2.6), with $\theta=\theta(\boldsymbol{F},\eta)$,

$$\frac{\partial U}{\partial\boldsymbol{F}}=\frac{\partial\Psi}{\partial\boldsymbol{F}}+\frac{\partial\Psi}{\partial\theta}\frac{\partial\theta}{\partial\boldsymbol{F}}+\eta\frac{\partial\theta}{\partial\boldsymbol{F}},\quad \frac{\partial U}{\partial\eta}=\frac{\partial\Psi}{\partial\theta}\frac{\partial\theta}{\partial\eta}+\eta\frac{\partial\theta}{\partial\eta}+\theta. \tag{2.12}$$

Then from (2.11), in terms of internal energy, stress and temperature obey

$$\boldsymbol{P}=\partial U/\partial\boldsymbol{F},\quad \theta=\partial U/\partial\eta. \tag{2.13}$$

Applying the polar decomposition to the deformation gradient,

$$\boldsymbol{F}=\boldsymbol{R}\boldsymbol{U}=\boldsymbol{V}\boldsymbol{R},\quad \boldsymbol{R}\boldsymbol{R}^{\mathrm{T}}=\boldsymbol{1},\quad \boldsymbol{U}=\boldsymbol{U}^{\mathrm{T}},\quad \boldsymbol{V}=\boldsymbol{V}^{\mathrm{T}}. \tag{2.14}$$

Let $\boldsymbol{C}=\boldsymbol{F}^{\mathrm{T}}\boldsymbol{F}=\boldsymbol{U}^2$. Material logarithmic strain $\boldsymbol{e}(\boldsymbol{X},t)$ is defined as

$$\boldsymbol{e}=\ln\boldsymbol{U}=\frac{1}{2}\ln\boldsymbol{C};\quad e_{IJ}=(\ln\boldsymbol{U})_{IJ}=e_{JI}. \tag{2.15}$$

General definitions, identities, and means of calculation of the logarithm of a second-order tensor are given in Jog (2008); in particular,

$$J=\sqrt{\det\boldsymbol{C}}=\exp(\mathrm{tr}\boldsymbol{e})=\exp(e_{KK}). \tag{2.16}$$

Free and internal energies (2.6) are now posited of the form

$$\Psi=\check{\Psi}(\boldsymbol{e},\theta),\quad U=\check{U}(\boldsymbol{e},\eta). \tag{2.17}$$

These seem to have been rarely used for anisotropic solids, an exception being analysis of higher-order moduli in Dłużewski (2000). Conjugate thermodynamic variables are

$$\check{\boldsymbol{S}}=\partial\check{\Psi}/\partial\boldsymbol{e}=\partial\check{U}/\partial\boldsymbol{e},\quad \eta=-\partial\check{\Psi}/\partial\theta,\quad \theta=\partial\check{U}/\partial\eta. \tag{2.18}$$

From (2.2), the first of (2.13), (2.15), and the chain rule, Cauchy stress is

$$\boldsymbol{\sigma}=J^{-1}\frac{\partial U}{\partial\boldsymbol{F}}\boldsymbol{F}^{\mathrm{T}}=J^{-1}\left(\frac{\partial U}{\partial\boldsymbol{C}}:\frac{\partial\boldsymbol{C}}{\partial\boldsymbol{F}}\right)\boldsymbol{F}^{\mathrm{T}}=2J^{-1}\boldsymbol{F}\frac{\partial U}{\partial\boldsymbol{C}}\boldsymbol{F}^{\mathrm{T}}=J^{-1}\boldsymbol{F}\left(\frac{\partial\check{U}}{\partial\boldsymbol{e}}:\frac{\partial\ln\boldsymbol{C}}{\partial\boldsymbol{C}}\right)\boldsymbol{F}^{\mathrm{T}}=J^{-1}\boldsymbol{F}(\check{\boldsymbol{S}}:\mathbf{M})\boldsymbol{F}^{\mathrm{T}}, \tag{2.19}$$

where Ψ can be used alternatively in place of U; in index notation,

$$\sigma_{ij}=J^{-1}F_{iK}F_{jL}\mathrm{M}_{IJKL}\check{S}_{IJ}. \tag{2.20}$$

Fourth-order tensor $\mathbf{M}$ obeys (Jog, 2008)

$$\mathbf{M}=\frac{\partial\ln\boldsymbol{C}}{\partial\boldsymbol{C}}=\sum_{i=1}^{3}\frac{1}{\Lambda_i}\boldsymbol{P}_i\boxtimes\boldsymbol{P}_i{}^{\mathrm{T}}+\sum_{i=1}^{3}\sum_{j=1;j\neq i}^{3}\frac{\ln\Lambda_i-\ln\Lambda_j}{\Lambda_i-\Lambda_j}\boldsymbol{P}_i\boxtimes\boldsymbol{P}_j^{\mathrm{T}}. \tag{2.21}$$

Here $\Lambda_i=\lambda_i^2$ are the principal values of $\boldsymbol{C}$, $(\boldsymbol{A}\boxtimes\boldsymbol{B})_{IJKL}=A_{IK}B_{JL}$, and

$$\boldsymbol{P}_i=\prod_{j=1;j\neq i}^{3}(\boldsymbol{C}-\Lambda_j\mathbf{1})/(\Lambda_i-\Lambda_j). \tag{2.22}$$

Noting that principal stretches λ_i are eigenvalues of $\boldsymbol{U}$ (and $\boldsymbol{V}$),

$$\boldsymbol{e}=\sum_{i=1}^{3}\boldsymbol{P}_i\ln\lambda_i=\frac{1}{2}\sum_{i=1}^{3}\boldsymbol{P}_i\ln\Lambda_i. \tag{2.23}$$

Let $c(\boldsymbol{e},\theta)$ denote specific heat per unit reference volume at constant deformation, where from (2.5) and (2.11):

$$c=\partial U/\partial\theta=\theta(\partial\eta/\partial\theta)=-\theta(\partial^2\Psi/\partial\theta^2). \tag{2.24}$$

The rate of internal energy can be expanded as

$$\dot{U}=(\partial U/\partial\boldsymbol{F}):\dot{\boldsymbol{F}}+(\partial U/\partial\eta)\dot{\eta}=\boldsymbol{P}:\dot{\boldsymbol{F}}+\theta[(\partial\eta/\partial\boldsymbol{F}):\dot{\boldsymbol{F}}+(\partial\eta/\partial\theta)\dot{\theta}]. \tag{2.25}$$

Substituting (2.24) and (2.25) into (2.7) leads to the temperature rate equation:

$$c\dot{\theta}=\theta(\partial^2\Psi/\partial\boldsymbol{F}\partial\theta):\dot{\boldsymbol{F}}-\nabla_0\cdot\boldsymbol{Q}. \tag{2.26}$$

Defining thermal stress coefficients $\check{\boldsymbol{\beta}}(\boldsymbol{e},\theta)$ as

$$\check{\boldsymbol{\beta}}=\partial\eta/\partial\boldsymbol{e}=-\partial\check{\boldsymbol{S}}/\partial\theta=-\partial^2\Psi/\partial\boldsymbol{e}\partial\theta, \tag{2.27}$$

(2.26) can be written as

$$c\dot{\theta}=-\theta\check{\boldsymbol{\beta}}:\dot{\boldsymbol{e}}-\nabla_0\cdot\boldsymbol{Q}=-c\theta\check{\boldsymbol{\Gamma}}:\dot{\boldsymbol{e}}-\nabla_0\cdot\boldsymbol{Q}. \tag{2.28}$$

The second-order tensor of Grüneisen parameters is

$$\check{\boldsymbol{\Gamma}}=\check{\boldsymbol{\beta}}/c. \tag{2.29}$$

The following Maxwell-type equalities can be derived using standard thermodynamic procedures like those in Thurston (1974) and Clayton (2011a):

$$\theta\check{\boldsymbol{\Gamma}}=(\theta/c)(\partial\eta/\partial\boldsymbol{e})=-\partial\check{\boldsymbol{S}}/\partial\eta=-\partial\theta/\partial\boldsymbol{e}, \tag{2.30}$$

$$(\theta/c^S)\check{\boldsymbol{\alpha}}=(\theta/c^S)(\partial\boldsymbol{e}/\partial\theta)=\partial\boldsymbol{e}/\partial\eta=-\partial\theta/\partial\check{\boldsymbol{S}}, \tag{2.31}$$

$$\check{\boldsymbol{\alpha}}=\partial\boldsymbol{e}/\partial\theta=\partial\eta/\partial\check{\boldsymbol{S}}. \tag{2.32}$$

Thermal expansion coefficients are $\check{\alpha}_{IJ}$. Specific heat at constant stress c^S obeys

$$c^S = \theta(\partial\eta/\partial\theta)|_{\boldsymbol{S}} = c + \theta\check{\boldsymbol{\alpha}} : \check{\boldsymbol{\beta}}. \tag{2.33}$$

Isothermal and isentropic second-order thermodynamic elastic coefficients are

$$\check{C}^{\theta}_{IJKL} = \left.\frac{\partial \check{S}_{KL}}{\partial e_{IJ}}\right|_{\theta} = \frac{\partial^2 \Psi}{\partial e_{IJ}\partial e_{KL}}, \quad \check{C}^{\eta}_{IJKL} = \left.\frac{\partial \check{S}_{KL}}{\partial e_{IJ}}\right|_{\eta} = \frac{\partial^2 U}{\partial e_{IJ}\partial e_{KL}}. \tag{2.34}$$

Thermal expansion and thermal stress coefficients are related by

$$\check{\boldsymbol{\beta}} = (\partial\eta/\partial\check{\boldsymbol{S}})|_{\theta} : (\partial\check{\boldsymbol{S}}/\partial\boldsymbol{e})|_{\theta} = \check{\boldsymbol{\alpha}} : \check{\mathbf{C}}^{\theta}; \quad \check{\beta}_{IJ} = \check{C}^{\theta}_{IJKL}\check{\alpha}_{KL}. \tag{2.35}$$

Isentropic and isothermal coefficients are related, using Maxwell relations, by

$$\check{\mathbf{C}}^{\eta} = (\partial\check{\boldsymbol{S}}/\partial\boldsymbol{e})|_{\theta} + (\partial\check{\boldsymbol{S}}/\partial\theta|_{\boldsymbol{e}}) \otimes (\partial\theta/\partial\boldsymbol{e})|_{\theta} = \check{\mathbf{C}}^{\theta} + (\theta/c)\check{\boldsymbol{\beta}} \otimes \check{\boldsymbol{\beta}}, \tag{2.36}$$

or in indicial notation,

$$\check{C}^{\eta}_{IJKL} = \check{C}^{\theta}_{IJKL} + (\theta/c)\check{\beta}_{IJ}\check{\beta}_{KL}. \tag{2.37}$$

Application is focused on wave propagation problems, for which the internal energy potential proves more convenient than the free energy potential. An unstrained reference state is defined by $(\boldsymbol{e}, \theta, \eta) = (\mathbf{0}, \theta_0, \eta_0)$; temperature and entropy changes from this reference state are $\Delta\theta = \theta - \theta_0$ and $\Delta\eta = \eta - \eta_0$. Greek subscripts denote Voigt notation for symmetric indices, e.g., $(\cdot)_{IJ} = (\cdot)_{JI} \leftrightarrow (\cdot)_{\alpha}$:

$$11 \leftrightarrow 1, \quad 22 \leftrightarrow 2, \quad 33 \leftrightarrow 3, \quad 23 = 32 \leftrightarrow 4, \quad 13 = 31 \leftrightarrow 5, \quad 12 = 21 \leftrightarrow 6. \tag{2.38}$$

Following standard convention (Clayton, 2011a; Thurston, 1974), shear strain components contain a factor of two, but stress and stiffness coefficients do not. For example, $e_6 = 2e_{12}, \check{S}_6 = \check{S}_{12}$, and $\check{C}_{66} = \check{C}_{1212}$. Internal energy per unit reference volume is expressed as a series expansion about energy U_0 from the reference state:

$$\check{U} = U_0 + \mathrm{C}_{\alpha}e_{\alpha} + \frac{1}{2!}\mathrm{C}_{\alpha\beta}e_{\alpha}e_{\beta} + \frac{1}{3!}\mathrm{C}_{\alpha\beta\gamma}e_{\alpha}e_{\beta}e_{\gamma} + \frac{1}{4!}\mathrm{C}_{\alpha\beta\gamma\delta}e_{\alpha}e_{\beta}e_{\gamma}e_{\delta} - \theta_0\left[\Gamma_{\alpha}e_{\alpha}\Delta\eta + \frac{1}{2!}\Gamma_{\alpha\beta}e_{\alpha}e_{\beta}\Delta\eta - h(\eta)\right]. \tag{2.39}$$

Letting $(\cdot)|_0 = (\cdot)|_{\boldsymbol{e}=\mathbf{0},\eta=\eta_0}$, material coefficients in (2.39) are constants evaluated at the reference state, which is prescribed stress free:

$$U_0 = \check{U}(\mathbf{0}, \eta_0), \quad \mathrm{C}_{\alpha} = (\partial\check{U}/\partial e_{\alpha})|_0 = 0; \tag{2.40}$$

$$\mathrm{C}_{\alpha\beta} = \left(\frac{\partial^2\check{U}}{\partial e_{\alpha}\partial e_{\beta}}\right)\bigg|_0, \quad \mathrm{C}_{\alpha\beta\gamma} = \left(\frac{\partial^3\check{U}}{\partial e_{\alpha}\partial e_{\beta}\partial e_{\gamma}}\right)\bigg|_0; \tag{2.41}$$

$$\begin{aligned} \theta_0\Gamma_{\alpha} &= \left(\frac{\theta}{c}\frac{\partial\eta}{\partial e_{\alpha}}\right)\bigg|_0 = -\left(\frac{\partial^2\check{U}}{\partial\eta\partial e_{\alpha}}\right)\bigg|_0, \\ \theta_0\Gamma_{\alpha\beta} &= \left(\theta\frac{\partial\check{\Gamma}_{\alpha}}{\partial e_{\beta}}\right)\bigg|_0 = -\left(\frac{\partial^3\check{U}}{\partial\eta\partial e_{\alpha}\partial e_{\beta}}\right)\bigg|_0. \end{aligned} \tag{2.42}$$

With constant specific heat $c_0 = (\partial U/\partial\theta)|_0$, to second order in entropy change,

$$h = c_0[\exp(\Delta\eta/c_0) - 1] \approx \Delta\eta + \frac{1}{2!}(\Delta\eta)^2/c_0. \tag{2.43}$$

Thermoelastic properties are usually reported in the context of conventional $\boldsymbol{E}$-based Lagrangian elasticity theory (Clayton, 2011a; Thurston, 1974; Wallace, 1972), where

$$\boldsymbol{E} = \frac{1}{2}(\boldsymbol{C} - \mathbf{1}) = \frac{1}{2}(\boldsymbol{F}^{\mathrm{T}}\boldsymbol{F} - \mathbf{1}), \quad U = \bar{U}(\boldsymbol{E}, \eta). \tag{2.44}$$

Let quantities with an overbar [i.e., $(\bar{\cdot})$] refer to those measured with respect to $\boldsymbol{E}$-based theory. It can be shown (Clayton, 2013; Dłużewski, 2000; Perrin & Delannoy-Coutris, 1983) that second-order isentropic elastic constants $\mathrm{C}_{\alpha\beta}$ and Grüneisen constants Γ_{α} should be equal when the reference state is unstressed for $\boldsymbol{E}$-based theory and $\boldsymbol{e}$-based (i.e., logarithmic) theory:

$$\mathrm{C}_{\alpha\beta} = \bar{\mathrm{C}}_{\alpha\beta}, \quad \Gamma_{\alpha} = \bar{\Gamma}_{\alpha}. \tag{2.45}$$

This result is consistent with the requirement that $\check{U} \approx \bar{U}$ when strains are small. Third-order isentropic constants are related, in full tensor notation, by Dłużewski (2000)

$$C_{IJKLMN} = \bar{C}_{IJKLMN} + 2(J_{IJKLPQ}C_{PQMN} + J_{KLMNPQ}C_{PQIJ} + J_{MNIJPQ}C_{PQKL}), \tag{2.46}$$

$$J_{IJKLMN} = \frac{1}{8}(\delta_{IK}\delta_{JM}\delta_{LN} + \delta_{IK}\delta_{JN}\delta_{LM} + \delta_{IL}\delta_{JM}\delta_{KN} + \delta_{IL}\delta_{JN}\delta_{KM} + \delta_{IM}\delta_{JK}\delta_{LN} + \delta_{IM}\delta_{JL}\delta_{KN} + \delta_{IN}\delta_{JK}\delta_{LM} + \delta_{IN}\delta_{JL}\delta_{KM}). \tag{2.47}$$

A standard assumption (Wallace, 1980) for weak shocks is $\rho\bar{\mathbf{\Gamma}} \approx$ constant, which yields (Clayton, 2013)

$$\bar{\Gamma}_{IJKL} = \frac{1}{2}(\partial\bar{\Gamma}_{IJ}/\partial E_{KL} + \partial\bar{\Gamma}_{KL}/\partial E_{IJ})|_0 \approx \frac{1}{2}(\Gamma_{IJ}\delta_{KL} + \Gamma_{KL}\delta_{IJ}), \tag{2.48}$$

Higher-order Grüneisen parameters $\Gamma_{\alpha\beta} \leftrightarrow \Gamma_{IJKL}$ are then related using the procedure outlined in Clayton (2013), giving

$$\Gamma_{IJKL} = \bar{\Gamma}_{IJKL} + \frac{1}{2}(\Gamma_{IK}\delta_{JL} + \Gamma_{JK}\delta_{IL} + \Gamma_{IL}\delta_{JK} + \Gamma_{JL}\delta_{IK}) \approx \frac{1}{2}(\Gamma_{IJ}\delta_{KL} + \Gamma_{KL}\delta_{IJ} + \Gamma_{IK}\delta_{JL} + \Gamma_{JK}\delta_{IL} + \Gamma_{IL}\delta_{JK} + \Gamma_{JL}\delta_{IK}). \tag{2.49}$$

2.2. Planar shock solution

A shock wave is represented as a propagating surface across which there may exist jump discontinuities in mass density, particle velocity, strain, stress, entropy, temperature, and internal energy. Considered here are 1-D (i.e, normal, planar, or longitudinal) shocks. Quantities associated with material ahead of the shock are denoted with superscript +, with material behind superscript −. In the present analysis of Section 2.2, material ahead of the shock is at rest, undeformed, unstressed, and at ambient reference temperature θ_0; these assumptions are removed later in Section 3.2. The jump in an arbitrary quantity $(\cdot)$ across the shock is written

$$[\![(\cdot)]\!] = (\cdot)^- - (\cdot)^+. \tag{2.50}$$

The shock moves at steady natural velocity $\mathfrak{D} > 0$ in the $X = X_1$ direction. The deformation gradient is

$$\boldsymbol{F}^- = [F_{ij}]^- = \begin{bmatrix} F & 0 & 0 \\ 0 & 1 & 0 \\ 0 & 0 & 1 \end{bmatrix} = \begin{bmatrix} 1+\xi & 0 & 0 \\ 0 & 1 & 0 \\ 0 & 0 & 1 \end{bmatrix}; \quad \boldsymbol{F}^+ = \mathbf{1}. \tag{2.51}$$

Behind the shock, with $x = x_1^-$ and $u = u_1^-$ particle coordinate and displacement,

$$F = \frac{\partial x}{\partial X} = 1 + \frac{\partial u}{\partial X} = 1 + \xi = J^- = \frac{V^-}{V_0} = \frac{\rho_0}{\rho^-}, \quad \xi = \partial u/\partial X. \tag{2.52}$$

Attention is restricted to compressive shocks, for which $0 < F \leqslant 1$ and $-1 < \xi \leqslant 0$. The only nonzero component of logarithmic strain $\boldsymbol{e}$ is

$$e = e_{11}^- = \ln F = \ln(1+\xi). \tag{2.53}$$

The "shock stress" or "shock pressure" is the longitudinal force per unit reference area (or equivalently, current area) behind the shock, positive in compression:

$$P = -P_{11}^- = -J(F_{1k}^{-1}\sigma_{1k})^- = -\sigma_{11}^-. \tag{2.54}$$

Let $\rho = \rho^-$ and $v = v_1^-$ be mass density and particle velocity in the shocked state. Conservation laws for mass, linear momentum, and energy – i.e., particular forms of the Rankine–Hugoniot equations – are, respectively (Clayton, 2013; McQueen et al., 1970; Thurston, 1974),

$$\rho_0\mathfrak{D} = \rho(\mathfrak{D} - v) \Longleftrightarrow \xi = -v/\mathfrak{D}, \tag{2.55}$$

$$P = \rho_0\mathfrak{D}v \;\Rightarrow\; \rho_0\mathfrak{D}^2 = -P/\xi \;\Longleftrightarrow\; \rho_0 v^2 = -P\xi, \tag{2.56}$$

$$Pv = \mathfrak{D}\left(\frac{1}{2}\rho_0 v^2 + [\![U]\!]\right) \;\Rightarrow\; [\![U]\!] = \frac{1}{2}\rho_0 v^2. \tag{2.57}$$

From (2.55), requiring $1 \geqslant J > 0$ leads to constraints $\mathfrak{D} > v \geqslant 0$. In (2.57), the usual adiabatic assumption of null heat conduction has been used. Shock compression is neither isothermal nor isentropic; the entropy inequality is (Germain & Lee, 1973)

$$[\![\eta/\rho_0]\!] \geqslant 0 \;\Rightarrow\; [\![\eta]\!] \geqslant 0. \tag{2.58}$$

Subsequent derivations invoke internal energy $U = \check{U}(\boldsymbol{e}, \eta)$ of (2.39). Derivatives of U with respect to strain depend only on entropy changes $\Delta\eta$ from the reference state and are independent of $\eta_0 = \eta^+$, and stress and temperature depend only on derivatives of internal energy with respect to strain and entropy and are independent of U_0. Therefore, let

$$U_0 = U^+ = 0, \quad \eta_0 = \eta^+ = 0 \;\Rightarrow\; [\![U]\!] = U^- = U, \quad [\![\eta]\!] = \eta^- = \Delta\eta = \eta; \tag{2.59}$$

$$\theta^+ = (\partial U/\partial\eta)^+ = \theta_0, \quad \theta^- = (\partial U/\partial\eta)^- = \theta \;\Rightarrow\; [\![\theta]\!] = \Delta\theta. \tag{2.60}$$

Stress components thermodynamically conjugate to e are related to P via (2.19), (2.21), (2.22) and (2.54), which reduce here to

$$P = -J^{-1}F_{1J}F_{1N}\check{S}_{KL}\mathsf{M}_{KLJN} = -F\check{S}_{11}\mathsf{M}_{1111} = -\check{S}/(1+\xi), \tag{2.61}$$

$$\check{S} = \check{S}_{11} = \partial\check{U}/\partial e_{11} = \partial\check{U}/\partial e, \tag{2.62}$$

where all quantites are evaluated behind the shock.

Expanding ξ and $(1+\xi)^{-1}$ in series to order five in logarithmic strain $e = e_{11}$,

$$\xi = \exp(e) - 1 \approx e + \frac{1}{2!}e^2 + \frac{1}{3!}e^3 + \frac{1}{4!}e^4 + \frac{1}{5!}e^5, \tag{2.63}$$

$$1/(1+\xi) \approx 1 - e + \frac{1}{2!}e^2 - \frac{1}{3!}e^3 + \frac{1}{4!}e^4 - \frac{1}{5!}e^5, \tag{2.64}$$

$$\xi/(1+\xi) \approx e - \frac{1}{2}e^2 + \frac{1}{6}e^3 - \frac{1}{24}e^4 + \frac{1}{120}e^5. \tag{2.65}$$

Using (2.56), (2.59), (2.61), and (2.65), balance (2.57) becomes, in terms of e,

$$U = -\frac{1}{2}P\xi = \frac{1}{2}\check{S}\xi/(1+\xi) \approx \frac{1}{2}\check{S}\left(e - \frac{1}{2}e^2 + \frac{1}{6}e^3 - \frac{1}{24}e^4 + \frac{1}{120}e^5\right). \tag{2.66}$$

Internal energy function (2.39) – using (2.43) and specialized to uniaxial strain with (2.53) and (2.59), to first order in entropy – becomes

$$\check{U}(e,\eta) = \frac{1}{2}\mathsf{C}_{11}e^2 + \frac{1}{6}\mathsf{C}_{111}e^3 + \frac{1}{24}\mathsf{C}_{1111}e^4 - \theta_0\left(\Gamma_1 e\eta + \frac{1}{2}\Gamma_{11}e^2\eta - \eta\right). \tag{2.67}$$

When $\check{U}$ is a linear function of entropy as in (2.67), then a solution for $\eta(e)$ can be obtained analytically in closed form, as in what follows. This form of internal energy is most valid for weak to moderate elastic shocks wherein $\eta/c_0 \ll 2$, which will be verified a posteriori in later examples. Conjugate thermodynamic stress is

$$\check{S} = \partial\check{U}/\partial e = \mathsf{C}_{11}e + \frac{1}{2}\mathsf{C}_{111}e^2 + \frac{1}{6}\mathsf{C}_{1111}e^3 - \theta_0(\Gamma_1 + \Gamma_{11}e)\eta. \tag{2.68}$$

This is substituted into (2.66), which then, when considered with (2.67), provides two equations in three unknowns (U, e, η). Writing $\eta(e)$ as a polynomial with constant coefficients $a_0, a_1, a_2, \ldots$,

$$\eta = a_0 + a_1 e + a_2 e^2 + a_3 e^3 + a_4 e^4 + a_5 e^5 + \cdots \tag{2.69}$$

Substituting (2.69) into (2.66) and (2.67), setting $U = \check{U}$, equating coefficients of like powers of e up to order five, and noting $\eta_0 = \eta(0) = 0$ from (2.59),

$$a_0 = a_1 = a_2 = 0, \quad a_3 = \frac{1}{12}\theta_0^{-1}(-3\mathsf{C}_{11} + \mathsf{C}_{111}), \tag{2.70}$$

$$a_4 = \frac{1}{24}\theta_0^{-1}[12\mathsf{C}_{11} - 6\mathsf{C}_{111} + \mathsf{C}_{1111} + \Gamma_1(-3\mathsf{C}_{11} + \mathsf{C}_{111})], \tag{2.71}$$

$$a_5 = \frac{1}{48}\theta_0^{-1}[-\mathsf{C}_{11} + 2\mathsf{C}_{111} - 2\mathsf{C}_{1111} + \Gamma_1(9\mathsf{C}_{11} - 5\mathsf{C}_{111} + \mathsf{C}_{1111}) + \Gamma_1^2(-3\mathsf{C}_{11} + \mathsf{C}_{111})]. \tag{2.72}$$

Substitution of entropy $\eta(e)$, now known to fifth order in strain, into (2.68) gives

$$\check{S}(e) = \mathsf{C}_{11}e + \frac{1}{2}\mathsf{C}_{111}e^2 + \left(\frac{1}{6}\mathsf{C}_{1111} - \theta_0\Gamma_1 a_3\right)e^3 - \theta_0(\Gamma_1 a_4 + \Gamma_{11}a_3)e^4 - \theta_0(\Gamma_1 a_5 + \Gamma_{11}a_4)e^5. \tag{2.73}$$

Use of this result for stress with (2.61) and Hugoniot equations (2.55)–(2.57) then gives shock pressure, internal energy, particle velocity, and shock velocity in terms of single variable $e = \ln J = \ln\frac{V}{V_0}$:

$$P = -\check{S}/\exp(e), \quad [\![U]\!] = \frac{1}{2}\check{S}[1 - \exp(-e)], \tag{2.74}$$

$$\upsilon = \{(\check{S}/\rho_0)[1 - \exp(-e)]\}^{1/2}, \tag{2.75}$$

$$\mathfrak{D} = \{(\check{S}/\rho_0)[1 - \exp(-e)]\}^{1/2}[1 - \exp(e)]. \tag{2.76}$$

Finally, thermoelastic temperature rise due to entropy production is simply

$$\theta = \partial\check{U}/\partial\eta = \theta_0\left(1 - \Gamma_1 e - \frac{1}{2}\Gamma_{11}e^2\right). \tag{2.77}$$

In the limit of very low shock stress, shock velocity approaches the longitudinal linear elastic wave speed

$$C_0 = (\mathsf{C}_{11}/\rho_0)^{1/2} \tag{2.78}$$

and shock stress in the first of (2.74) approaches the isentrope

$$P^{\eta} = -\exp(-e)\left(C_{11}e + \frac{1}{2}C_{111}e^2 + \frac{1}{6}C_{1111}e^3\right). \tag{2.79}$$

2.3. Results: elastic solution

Theory and analytical solutions derived in Section 2.2 are now applied to analyze shock compression behavior of single crystals of three hard minerals: sapphire (α-Al_2O_3 or corundum), diamond (C), and quartz (α-SiO_2). These materials are considered because elastic deformations in excess of several percent volumetric compression can be achieved in uniaxial compression prior to any inelastic deformation that could render the analysis of Section 2.2 unrealistic. These materials also belong to the limited set of anisotropic crystals whose complete third-order, and in some cases fourth-order, elastic constants have been reported.

Analytical solutions are studied for uniaxial shock compression involving internal energy function (2.39) incorporating logarithmic strain $\boldsymbol{e}$ with elastic constants up to possibly fourth order. Certain results are also compared with those obtained previously (Clayton, 2013) for Lagrangian ($\boldsymbol{E}$-based) and Eulerian ($\boldsymbol{D}$-based) nonlinear thermoelastic models. Sapphire and quartz have trigonal (i.e., rhombohedral) symmetry and are analyzed for compression along two pure mode directions: the a-axis (X-cut, $[\bar{1}2\bar{1}0]$) and c-axis (Z-cut, [0001]). The b-axis is not a pure mode direction in trigonal crystals; the plane wave approximation used for analysis of Y-cut quartz in Clayton (2013), which omits possible transverse displacements, is not repeated herein. Diamond is cubic and is analyzed for pure mode compression along a cube axis (X-cut, [100]). Elastic constants are interchanged as needed for consistency with notation of Section 2.2. For example, for c-axis (i.e., Z-cut) compression, C_{11} is replaced by C_{33}, C_{111} by C_{333}, Γ_1 by Γ_3, etc.

Thermoelastic properties are listed in Table 1. Second-order elastic constants are reported from ultrasonic experiments (McSkimin, Andreatch, & Glynn, 1972; McSkimin, Andreatch, & Thurston, 1965; Winey, Gupta, & Hare, 2001). Higher-order constants are converted from reported Lagrangian values (Hankey & Schuele, 1970; Nielsen, 1986; Thurston et al., 1966) to logarithmic values via (2.46) and (2.49). Complete sets of anisotropic second- and third-order constants are listed for later

Table 1
Thermoelastic single crystal properties ($\theta_0 = 295$ K; $C_{\alpha\beta\ldots}$ in GPa).

Property	Sapphire	Diamond	Quartz
C_{11}	498	1079	88
C_{12}	163	124	7
C_{13}	117	C_{12}	12
C_{14}	23	–	−18
C_{33}	502	C_{11}	106
C_{44}	147	578	58
C_{111}	−792	174	315
C_{112}	−764	−552	−331
C_{113}	−729	C_{112}	36
C_{114}	−9	–	−199
C_{123}	−289	0	−294
C_{124}	62	–	−33
C_{133}	−688	C_{112}	−288
C_{134}	154	–	−16
C_{144}	−162	124	−125
C_{155}	−559	−843	−34
C_{222}	−1532	C_{111}	193
C_{333}	−328	C_{111}	−181
C_{344}	−487	C_{155}	65
C_{444}	−16	–	−249
C_{456}	$\frac{1}{2}(C_{155} - C_{144})$	−433	$\frac{1}{2}(C_{155} - C_{144})$
C_{1111}	–	–	10^4
C_{3333}	–	–	10^4
Γ_1	1.29	0.81	0.74
Γ_3	1.29	Γ_1	0.58
Γ_{11}	3.87	2.43	2.22
Γ_{12}	1.29	0.81	0.74
Γ_{13}	1.29	Γ_{12}	0.66
Γ_{33}	3.87	Γ_{11}	1.74
B_0	254	442	38
G_0	166	538	48
B_0'	4.3	4.0	6.3
ρ_0 [g/cm^3]	3.98	3.51	2.65
c_0 [MPa/K]	3.10	1.73	1.95
P_H/C_{11}	0.05	0.08	0.10

use in Section 3.3; in fact, only longitudinal constants are needed presently for analysis of the axial purely thermoelastic response, as is clear from the solution derived in Section 2.2. Bulk modulus B_0 and its pressure derivative B_0' (Gieske & Barsch, 1968; McSkimin & Andreatch, 1972; McSkimin et al., 1965) are also listed; these enter the hydrostatic EOS described in the Appendix A. For crystals with cubic symmetry,

$$B_0 = \frac{1}{3}(C_{11} + 2C_{12}), \tag{2.80}$$

while for crystals with trigonal or hexagonal symmetry,

$$B_0 = \left[(C_{11} + C_{12})C_{33} - 2C_{13}^2\right]/[C_{11} + C_{12} + 2C_{33} - 4C_{13}]. \tag{2.81}$$

Constant B_0' is formally related to combinations of second- and third-order elastic constants (Guinan & Steinberg, 1974), but is often measured directly or fit to high pressure data. Also listed for each crystal is the Voigt-average shear modulus G_0, used later in Section 3 for normalization of shear strength. For crystals with cubic symmetry,

$$G_0 = \frac{1}{5}(C_{11} - C_{12} + 3C_{44}), \tag{2.82}$$

while for crystals with trigonal or hexagonal symmetry,

$$G_0 = \frac{1}{15}\left\{[2C_{11} + C_{33}] - [C_{12} + 2C_{13}] + 3\left[\frac{1}{2}(C_{11} - C_{12}) + 2C_{44}\right]\right\}. \tag{2.83}$$

As discussed later, fourth-order constants C_{1111} and C_{3333} for quartz are fit to shock velocity versus particle velocity data (Fowles, 1967), but these are not needed for sapphire or diamond described with logarithmic elastic theory. Maximum HEL stresses P_H from shock experiments (Graham, 1972; Fowles, 1967; Lang & Gupta, 2010; Wackerle, 1962) are shown for reference, normalized by second-order moduli (X-cut shown). The domain of validity of elastic analysis can be estimated as $\frac{V}{V_0} \gtrsim \frac{C_{11}-P_H}{C_{11}}$. In sapphire, the elastic domain for Z-cut quartz is about the same as that for X-cut (Graham, 1972; Graham & Brooks, 1971); in quartz, the elastic domain for Z-cut is demarcated by $\frac{P_H}{C_{33}} \approx 0.15$ (Fowles, 1967; Wackerle, 1962).

Predicted shock velocity $\mathfrak{D}$ versus particle velocity v is compared with experimental shock compression data of Graham and Brooks (1971) in Fig. 1a for X- and Z-cut sapphire. Experimental data are obtained from flyer-plate and explosive loading configurations; in the latter, two-wave structures arose (Graham & Brooks, 1971). Data considered here correspond only to the elastic shock, with the secondary, slower "plastic" wave in which the HEL was exceeded not addressed here; the plastic response will be modeled in Section 3. Velocities are normalized by wave speed (2.78). Predictions marked "3rd order" are obtained using complete solutions and all material constants in Table 1. Predictions marked "2nd order" assume $C_{111} = 0$. Note that fourth-order constant C_{1111} is not needed for either orientation (Table 1). Considering scatter in the data, 3rd order and 2nd order fits are adequate for each orientation, giving nearly linear $\mathfrak{D}$-v curves over the compression range for which sapphire remains elastic ($\frac{V}{V_0} \gtrsim 0.95$). Second order predictions for X- and Z-cut orientations are almost identical and correspond to the broken line with lowest slope in Fig. 1(a). Hugoniot stress (i.e., P) normalized by C_{11} or C_{33} is shown in Fig. 1(b) and (c), along with experimental data (Graham & Brooks, 1971). Also shown are 2nd order predictions made using analytical solutions given in Clayton (2013) for Lagrangian $\boldsymbol{E}$-based theory and Eulerian $\boldsymbol{e}$-based theory. For each orientation, 2nd and 3rd order logarithmic model predictions provide close agreement with experiment. The other nonlinear elastic models (Clayton, 2013) are comparatively inaccurate, with 2nd order Eulerian theory too stiff and 2nd order Lagrangian theory too compliant.

Predictions of normalized shock velocity and Hugoniot stress in diamond are given in Fig. 2(a) and (b), respectively, compared with experimental data of Lang and Gupta (2010). Fourth-order constant C_{1111} is not needed. From Fig. 2(a), differences in 2nd and 3rd order predictions of logarithmic theory are small, with both providing close agreement with experimental velocity data. Likewise in Fig. 2(b), differences in 2nd and 3rd order predictions of logarithmic theory are small, with both providing close agreement with experimental stress data. The other 2nd order elastic models (Clayton, 2013) do not accurately predict Hugoniot stress, with 2nd order Eulerian theory too stiff and 2nd order Lagrangian theory too compliant.

Predicted shock velocity $\mathfrak{D}$ versus particle velocity v is compared with experimental shock compression data of Fowles (1967) in Fig. 3a for X- and Z-cut quartz. Experimental data are obtained from plane-wave explosive loading (Fowles, 1967); data considered here correspond only to the first, elastic shock in each test. Fourth-order constant C_{1111} was fit to the data in Fowles (1967). Predictions marked "3rd order" assume $C_{1111} = 0$. Predictions of shock stress are compared with those of 3rd order Lagrangian and Eulerian nonlinear elastic solutions (Clayton, 2013) in Fig. 3(b). For each orientation, 4th order theories are required to most accurately match the experimental Hugoniot data; 2nd and 3rd order models are all too compliant. However, 3rd order logarithmic theory more closely matches the data for Z-cut quartz than 3rd order Lagrangian and Eulerian theories.

Predictions of the present logarithmic nonlinear thermoelasticity theory for temperature rise θ (normalized by reference temperature θ_0), entropy jump across the shock η (normalized by specific heat c_0), and Hugoniot stress P (normalized by uniaxial isentropic stress P^{η}) are listed in Table 2. Temperatures are computed from (2.77), entropy from (2.69), and isentropes from (2.79), for each crystal with the full set of material properties given in Table 1. Predicted temperature rise is fairly small for elastic shock loading, similar to results reported for Lagrangian and Eulerian theories in Clayton (2013). Entropy is positive in agreement with (2.58) and is of the same order of magnitude reported for Lagrangian and Eulerian theories in Clayton

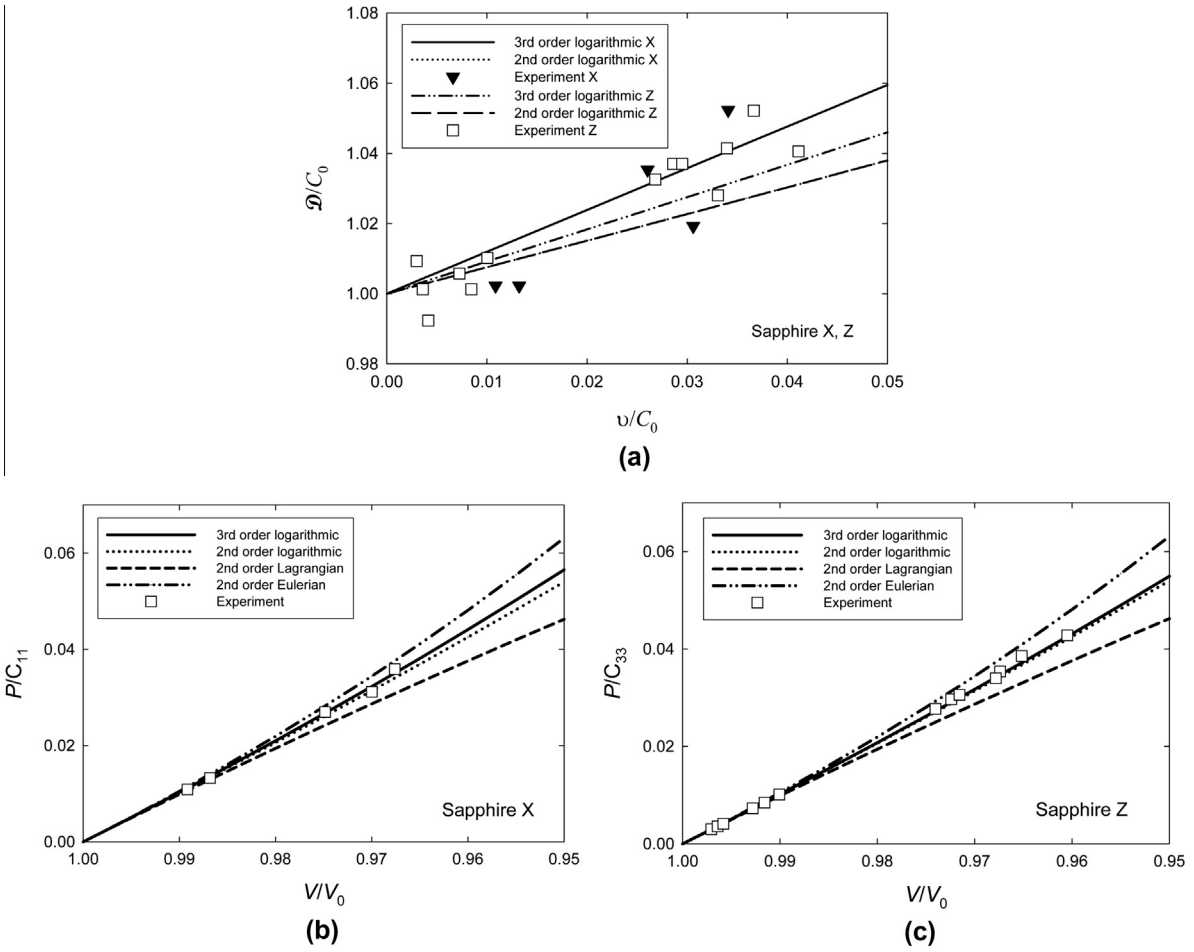

Fig. 1. Analytical nonlinear elastic solutions and experimental data (Graham & Brooks, 1971) for sapphire: (a) shock velocity vs. particle velocity, X- and Z-cut (b) shock stress vs. volume ratio, X-cut (c) shock stress vs. volume ratio, Z-cut.

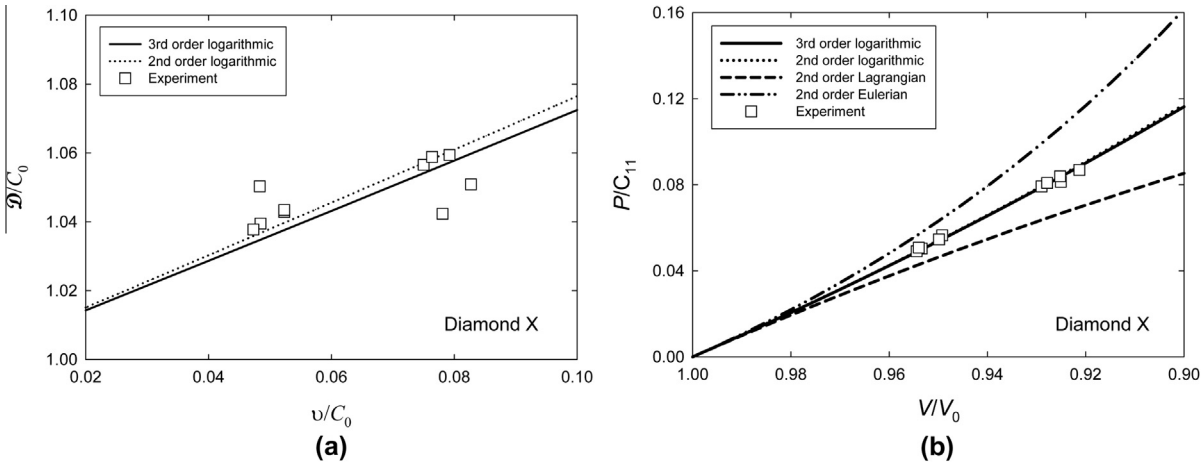

Fig. 2. Analytical nonlinear elastic solutions and experimental data (Lang & Gupta, 2010) for diamond: (a) shock velocity vs. particle velocity, X-cut (b) shock stress vs. volume ratio, X-cut.

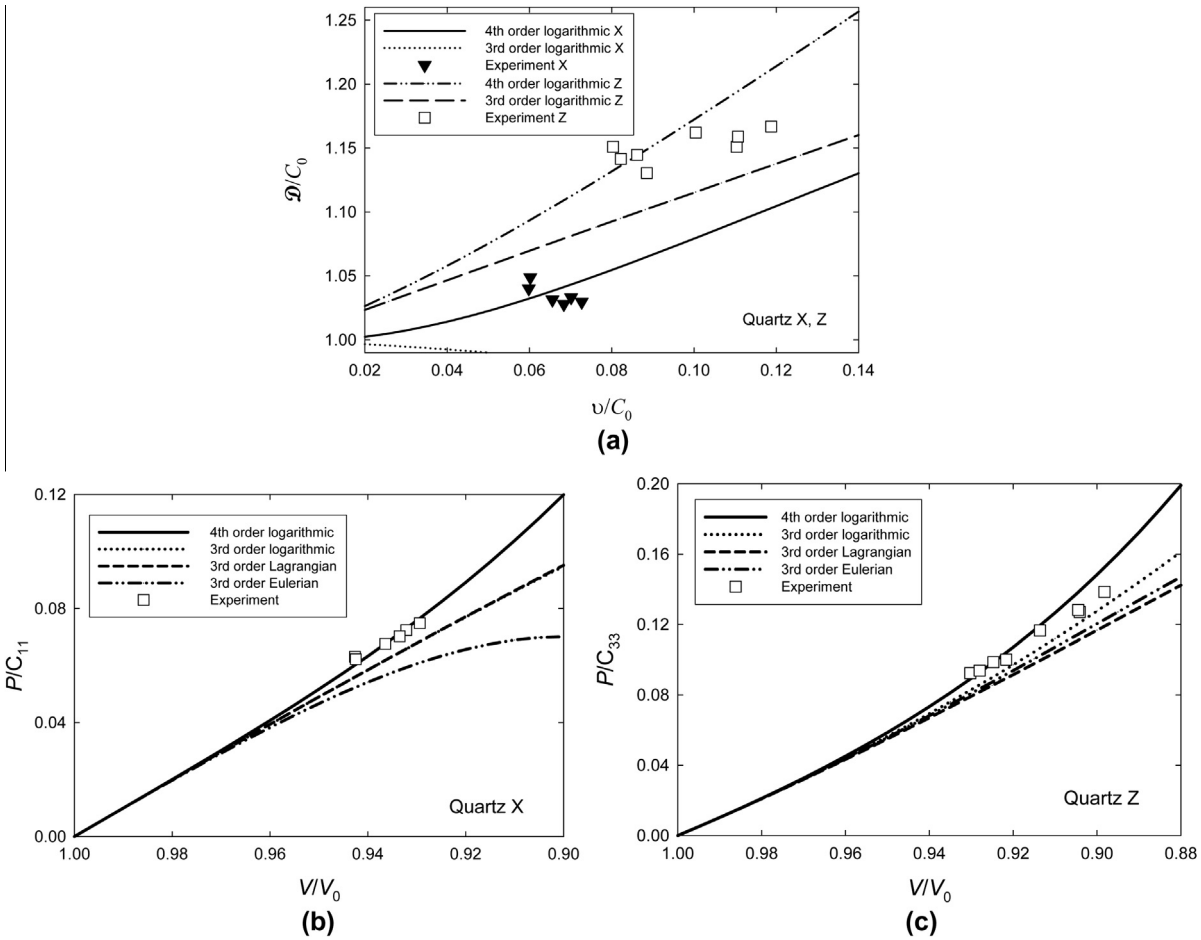

Fig. 3. Analytical nonlinear elastic solutions and experimental data (Fowles, 1967) for quartz: (a) shock velocity vs. particle velocity, X- and Z-cut (b) shock stress vs. volume ratio, X-cut (c) shock stress vs. volume ratio, Z-cut.

Table 2
Thermodynamic predictions of nonlinear logarithmic theory.

Material	Direction	V/V_0	θ/θ_0	η/c_0	P/P^{η}
Sapphire	X	0.96	1.049	0.016	1.0008
		0.92	1.094	0.145	1.0028
		0.88	1.133	0.556	1.0056
	Z	0.96	1.049	0.012	1.0006
		0.92	1.094	0.110	1.0022
		0.88	1.133	0.420	1.0045
Diamond	X	0.96	1.031	0.036	1.0003
		0.92	1.059	0.327	1.0011
		0.88	1.083	1.248	1.0023
Quartz	X	0.96	1.028	0.001	1.0002
		0.92	1.054	0.030	1.0013
		0.88	1.076	0.178	1.0041
	Z	0.96	1.022	0.007	1.0005
		0.92	1.042	0.086	1.0021
		0.88	1.060	0.400	1.0046

(2013). Recall from Section 2.2 that the present analytical solution assumes the contribution to internal energy from entropy is linear in (2.67), most accurate for $\eta \ll 2c_0$. From Table 2, such conditions hold for $\frac{V}{V_0} \geqslant 0.92$. Examination of stresses in Table 2 shows that $\frac{P}{P^{\eta}} < 1.01$ in all cases, meaning an isentropic assumption for elastic shock compression is accurate for predicting axial stress up to the HEL in these crystals. Values listed in Table 2 are considered extrapolations when compression

exceeds the HEL. Above the HEL, a nonlinear thermoelastic–plastic theory incorporating inelastic deformation mechanisms and associated dissipation, as developed and applied next in Section 3, becomes necessary.

3. Anisotropic logarithmic thermoelastic–plastic theory

3.1. Continuum theory

Assuming again that $\boldsymbol{x}$ is differentiable, deformation gradient (2.1) is decomposed multiplicatively (Clayton, 2011a; Teodosiu & Sidoroff, 1976) as

$$\boldsymbol{F} = \nabla_0 \boldsymbol{x} = \boldsymbol{F}^{\mathrm{E}}\boldsymbol{F}^{\mathrm{P}}; \quad F_{iJ} = \partial_J x_i = F^{\mathrm{E}}_{ik}F^{\mathrm{P}}_{Kj}. \tag{3.1}$$

Here $\boldsymbol{F}^{\mathrm{E}}$ and $\boldsymbol{F}^{\mathrm{P}}$ denote deformation "gradient" mappings associated with thermoelasticity and defects (e.g., dislocation slip, twinning, or cleavage fracture), though neither generally anholonomic mapping (Clayton, 2012) need be compatible (i.e., a true gradient of a vector field). Each is, however, presumed to have positive determinant: $J^{\mathrm{E}} = \det \boldsymbol{F}^{\mathrm{E}} > 0$ and $J^{\mathrm{P}} = \det \boldsymbol{F}^{\mathrm{P}} > 0$. The usual stress definitions and local balance laws of continuum mechanics of Section 2.1 still apply [(2.2), (2.3), (2.4), (2.7), and (2.8)], again here assuming no body forces or scalar heat sources.

Logarithmic thermoelastic strain is now defined as (no "E" superscript)

$$\boldsymbol{e} = \ln \boldsymbol{U}^{\mathrm{E}} = \frac{1}{2}\ln \boldsymbol{C}^{\mathrm{E}}, \tag{3.2}$$

where the polar decomposition $\boldsymbol{F}^{\mathrm{E}} = \boldsymbol{R}^{\mathrm{E}}\boldsymbol{U}^{\mathrm{E}}$, and $\boldsymbol{C}^{\mathrm{E}} = \boldsymbol{F}^{\mathrm{ET}}\boldsymbol{F}^{\mathrm{E}}$. Analogously to (2.16), thermoelastic volume change obeys $J^{\mathrm{E}} = \exp(\mathrm{tr}\boldsymbol{e})$.

Let ξ represent a generic internal state variable associated with evolution of microstructure, for example, dislocation or crack density. Here, ξ is assumed scalar, but generalization to higher-order tensors (Bammann, 1984) poses no theoretical difficulties. Assuming uniform properties in the reference state, free and internal energy densities per unit initial volume are of the form

$$\Psi = \check{\Psi}(\boldsymbol{e}, \theta, \xi), \quad U = \check{U}(\boldsymbol{e}, \eta, \xi), \tag{3.3}$$

related as usual via $U = \Psi + \theta\eta$. Define thermodynamic conjugate forces as

$$\check{\boldsymbol{S}} = \partial\check{U}/\partial\boldsymbol{e}, \quad \zeta = -\partial\check{U}/\partial\xi. \tag{3.4}$$

Using (2.7), (2.8), (3.3), and (3.4), and considering admissible thermomechanical processes, the following constitutive laws can be derived consistently with the first and second laws of thermodynamics (see e.g., Clayton, 2011a):

$$\boldsymbol{\sigma} = J^{\mathrm{E}-1}\boldsymbol{F}^{\mathrm{E}}(\check{\boldsymbol{S}} : \mathsf{M})\boldsymbol{F}^{\mathrm{ET}}, \quad \eta = -\partial\check{\Psi}/\partial\theta, \quad \theta = \partial\check{U}/\partial\eta. \tag{3.5}$$

Here, $\mathsf{M} = \partial \ln \boldsymbol{C}^{\mathrm{E}}/\partial\boldsymbol{C}^{\mathrm{E}}$ is computed analogously to (2.21). With $\boldsymbol{L}^{\mathrm{P}}$ the inelastic velocity gradient, entropy inequality (2.8) reduces to

$$J\boldsymbol{\sigma} : (\boldsymbol{F}^{\mathrm{E}}\boldsymbol{L}^{\mathrm{P}}\boldsymbol{F}^{\mathrm{E}-1}) + \zeta\dot{\xi} - \boldsymbol{Q}\cdot\nabla_0\theta \geqslant 0; \quad (\boldsymbol{L}^{\mathrm{P}} = \dot{\boldsymbol{F}}^{\mathrm{P}}\boldsymbol{F}^{\mathrm{P}-1}). \tag{3.6}$$

Defining specific heat at constant elastic strain as in (2.24), i.e., $c = \partial U/\partial\theta = -\theta\partial^2\Psi/\partial\theta^2$, the balance of energy becomes

$$c\dot{\theta} = J\boldsymbol{\sigma} : (\boldsymbol{F}^{\mathrm{E}}\boldsymbol{L}^{\mathrm{P}}\boldsymbol{F}^{\mathrm{E}-1}) + \theta(\partial\check{\boldsymbol{S}}/\partial\theta) : \dot{\boldsymbol{e}} + [\zeta - \theta(\partial\zeta/\partial\theta)]\dot{\xi} - \nabla_0\cdot\boldsymbol{Q}. \tag{3.7}$$

Generic kinetic equations for inelasticity are of the state-dependent form

$$\boldsymbol{L}^{\mathrm{P}} = \boldsymbol{L}^{\mathrm{P}}(\boldsymbol{F}^{\mathrm{E}}, \eta, \xi), \quad \dot{\xi} = \dot{\xi}(\boldsymbol{F}^{\mathrm{E}}, \eta, \zeta). \tag{3.8}$$

Thermodynamic definitions and identities in (2.27) and 2.29, (2.30)–(2.36) and (2.37) still apply in the elastic–plastic case, where now it is understood that $\boldsymbol{e}$ is the thermoelastic part of the total strain as in (3.2).

For anisotropic single crystal plasticity, contributions to inelastic deformation can often be attributed to deformation on distinct planes with reference unit normal vector $\boldsymbol{m}_0^\alpha$, in unit reference direction $\boldsymbol{s}_0^\alpha$, where $\alpha = 1, 2, \ldots, n$, with n the number of possible deformation systems. Let $\dot{\gamma}^\alpha$ denote the scalar deformation rate on system α, which in general here can be due to dislocation glide, deformation twinning, or cleavage fracture. The inelastic velocity gradient and inelastic dilatation rate become

$$\boldsymbol{L}^{\mathrm{P}} = \sum_\alpha \dot{\gamma}^\alpha \boldsymbol{s}_0^\alpha \otimes \boldsymbol{m}_0^\alpha, \quad \dot{J}^{\mathrm{P}} = J^{\mathrm{P}}\sum_\alpha \dot{\gamma}^\alpha \boldsymbol{s}_0^\alpha \cdot \boldsymbol{m}_0^\alpha. \tag{3.9}$$

Lattice directors deform thermoelastically via

$$\boldsymbol{s}^\alpha = \boldsymbol{F}^{\mathrm{E}}\boldsymbol{s}_0^\alpha, \quad \boldsymbol{m}^\alpha = \boldsymbol{F}^{\mathrm{E}-\mathrm{T}}\boldsymbol{m}_0^\alpha. \tag{3.10}$$

Let $\gamma^\alpha = \int \dot{\gamma}^\alpha \mathrm{d}t$ denote the cumulative deformation on system α over a time increment in which deformation increases monotonically. For dislocation glide, γ^α then represents isochoric plastic shear ($\boldsymbol{s}_0^\alpha \cdot \boldsymbol{m}_0^\alpha = 0$); for twinning, $\gamma^\alpha = \gamma_{\mathrm{T}} f^\alpha$, with

f^α and γ_T the local volume fraction of twinned crystal and characteristic twinning shear (Clayton, 2009, 2010c) (twinning is likewise isochoric with $\boldsymbol{s}_0^\alpha \cdot \boldsymbol{m}_0^\alpha = 0$). For cleavage (Clayton, 2010b), mode II/III fracture is isochoric ($\boldsymbol{s}_0^\alpha \cdot \boldsymbol{m}_0^\alpha = 0$), but mode I is not ($\boldsymbol{s}_0^\alpha \cdot \boldsymbol{m}_0^\alpha = 1$ and $\gamma^\alpha \geqslant 0$.) Dislocation glide is lattice preserving and does not affect thermoelastic properties such as elastic moduli. Deformation twinning induces lattice rotation that can affect moduli and slip directors within twinned regions. Fractures may induce degradation of thermoelastic properties.

Using (3.9) and (3.10), dissipation (3.6) and temperature rate (3.7) become

$$\sum_\alpha \tau^\alpha \dot{\gamma}^\alpha + \zeta\xi - \mathbf{Q} \cdot \nabla_0 \theta \geqslant 0, \quad (\tau^\alpha = J\boldsymbol{\sigma} : \boldsymbol{s}^\alpha \otimes \boldsymbol{m}^\alpha); \tag{3.11}$$

$$c\dot{\theta} = \sum_\alpha \tau^\alpha \dot{\gamma}^\alpha + \theta(\partial \check{\mathbf{S}}/\partial\theta) : \dot{\boldsymbol{e}} + [\zeta - \theta(\partial\zeta/\partial\theta)]\dot{\xi} - \nabla_0 \cdot \mathbf{Q}. \tag{3.12}$$

The thermodynamic driving force for inelastic deformation on system α is resolved Kirchhoff stress τ^α. For rate dependent inelasticity, a more specific form of the first of (3.8) is

$$\dot{\gamma}^\alpha = \dot{\gamma}^\alpha(\tau^\alpha, \theta, \xi). \tag{3.13}$$

In the rate independent limit, often thought adequate for describing strong crystals such as ceramics whose shearing resistance g^α is an appreciable fraction of the theoretical strength (Graham & Brooks, 1971), (3.13) is replaced with

$$\tau^\alpha < g^\alpha(\theta, \xi) \iff \dot{\gamma}^\alpha = 0, \quad \tau^\alpha = g^\alpha(\theta, \xi) \iff |\dot{\gamma}^\alpha| \geqslant 0. \tag{3.14}$$

Rate independent theory also proves useful as a limiting case for describing the response in problems such as shock compression wherein the true strain rate is unspecified or unknown (e.g., a shock represented mathematically as a moving surface of discontinuity, as in Germain & Lee (1973), Perrin & Delannoy-Coutris (1983) and in later Section 3.2 of the present work).

Application is again focused on wave propagation problems. Internal energy per unit reference volume is expressed as a series expansion about energy U_0 from the reference state as in (2.39)–(2.42) and (2.43):

$$\check{U} = U_0 + \frac{1}{2}\mathsf{C}_{\alpha\beta}e_\alpha e_\beta + \frac{1}{6}\mathsf{C}_{\alpha\beta\gamma}e_\alpha e_\beta e_\gamma + \frac{1}{24}\mathsf{C}_{\alpha\beta\gamma\delta}e_\alpha e_\beta e_\gamma e_\delta + \theta_0\Delta\eta\left[1 + \frac{1}{2c_0}\Delta\eta - \Gamma_\alpha e_\alpha - \frac{1}{2}\Gamma_{\alpha\beta}e_\alpha e_\beta\right] + \frac{1}{2}\kappa \mathsf{G}_0 \xi^2. \tag{3.15}$$

The final term represents stored energy of lattice defects for example, Regueiro, Bammann, Marin, and Garikipati (2002) and Clayton (2005a), with $\kappa = \frac{1}{\mathsf{G}_0}\frac{\partial^2 U}{\partial \xi^2}$ a dimensionless constant. Here, isentropic moduli are generally anisotropic but constant as in Section 2.1; for simplicity, possible effects of twinning or damage on elastic moduli are omitted. Identities in (2.45)–(2.48) and (2.49) still apply.

3.2. Planar shock solution

Consider a continuous and initially homogeneous slab of material through which a planar shock moves, in the x_1-direction, with natural velocity $\mathfrak{D}$. As in Section 2.2, let superscripts + and − label quantities in the material ahead (i.e., upstream) and behind (i.e., downstream) from the shock. Let $[\![(\cdot)]\!] = (\cdot)^- - (\cdot)^+$ and $\langle(\cdot)\rangle = \frac{1}{2}[(\cdot)^- + (\cdot)^+]$ denote the jump and average of a quantity across the shock. Let $\boldsymbol{n}$ be a unit normal vector to the planar shock, i.e., $\boldsymbol{n} = \partial\boldsymbol{x}/\partial x_1$. The only nonvanishing component of particle velocity is $v = \boldsymbol{v} \cdot \boldsymbol{n}$. The Cauchy stress component normal to the shock front is $\sigma = \boldsymbol{\sigma} : (\boldsymbol{n} \otimes \boldsymbol{n}) = \sigma_{11}$. The relative velocity of the material with respect to the shock is $\mathsf{v} = v - \mathfrak{D}$. Let $u = U/\rho_0$ denote internal energy per unit mass. Appropriate forms of the Rankine–Hugoniot conditions for conservation of mass, momentum, and energy are (Germain & Lee, 1973)

$$[\![\rho\mathsf{v}]\!] = 0, \tag{3.16}$$

$$[\![\sigma]\!] - \rho\mathsf{v}[\![\mathsf{v}]\!] = 0, \tag{3.17}$$

$$[\![\rho\mathsf{v}\left(u + \frac{1}{2}\mathsf{v}^2\right) - \sigma\mathsf{v}]\!] = 0. \tag{3.18}$$

The material need not be deformed uniaxially according to these conditions, but shock velocity and particle velocity must both be rectilinear in the x_1-direction so that only normal traction is discontinuous. Therefore, these equations can apply for shock(s) passing through a pre-stressed material such as a plastic wave following an elastic precursor, making them more general than 2.55, 2.56 and 2.57 of Section 2.2 that apply only for a single shock passing through an initially unstressed slab. Adiabatic conditions have been assumed (Germain & Lee, 1973): $\mathbf{Q} = \mathbf{0}$, leading to entropy production requirement (2.58). Using (3.16) and (3.17), energy conservation condition (3.18) can be rewritten as (Germain and Lee, 1973)

$$[\![u]\!] = \langle\sigma\rangle[\![1/\rho]\!] \iff [\![U]\!] = \langle\sigma\rangle[\![J]\!]. \tag{3.19}$$

Assume that the upstream state and shock velocity are known. The downstream state is defined by variables $(v^-, \rho^-, \sigma^-, u^-)$. The Rankine–Hugoniot conditions provide three equations for determining this state; in order to fully obtain the downstream state, a fourth equation is supplied by the constitutive model, or another downstream variable must be known. For example, in experiments particle velocity v^- is often measured in addition to $\mathfrak{D}$.

Considered in what follows are longitudinal elastic–plastic shocks corresponding to planar impact in pure mode directions in single crystals (i.e., directions parallel to an axis of threefold or greater symmetry). A sample of material subjected to a step or ramp loading in normal stress along this direction, with no applied shear stress, develops a two-wave structure consisting of a single longitudinal elastic wave (i.e., the elastic precursor), followed by a single longitudinal plastic wave if the HEL is exceeded. Implicitly, overdriven shocks in which the plastic wave overtakes the elastic precursor are not considered. Total deformation is thus

$$\boldsymbol{F}^{+}=\begin{bmatrix} F^{+} & 0 & 0\\ 0 & 1 & 0\\ 0 & 0 & 1\end{bmatrix}=[F^{\mathrm{E}}_{ij}]^{+},\quad \boldsymbol{F}^{-}=\begin{bmatrix} F^{-} & 0 & 0\\ 0 & 1 & 0\\ 0 & 0 & 1\end{bmatrix}=[F^{\mathrm{E}}_{iK}F^{\mathrm{P}}_{KJ}]^{-}, \tag{3.20}$$

where hereafter superscripts + and − label quantities in front of and behind the plastic shock, i.e., at the HEL state of the elastic precursor and the final inelastic state. Note that at the HEL state, $\boldsymbol{F}^{+}=(\boldsymbol{F}^{\mathrm{E}})^{+}$, while behind the shock, $\boldsymbol{F}^{-}=(\boldsymbol{F}^{\mathrm{E}}\boldsymbol{F}^{\mathrm{P}})^{-}$. For crystal orientations of lower symmetry, or if shear stress is applied in addition of longitudinal pressure, quasi-longitudinal and multiple quasi-transverse elastic and plastic waves would appear (Johnson, 1972); such more complicated problems, for which (3.20) no longer applies, are not addressed herein.

For the highly symmetric orientations considered in detail for sapphire and diamond in Section 3.3, n inelastic shear systems are active simultaneously at shock stresses exceeding P_{H}, all at the same rate $\dot{\gamma}=\dot{\gamma}^{\alpha}$. For monotonic loading, integration of (3.9) yields the plastic deformation, to order three in γ:

$$\boldsymbol{F}^{\mathrm{P}}(\gamma)=\exp\left(\gamma\sum_{\alpha}\boldsymbol{s}^{\alpha}_{0}\otimes\boldsymbol{m}^{\alpha}_{0}\right)\approx\boldsymbol{1}+\gamma\sum_{\alpha}\boldsymbol{s}^{\alpha}_{0}\otimes\boldsymbol{m}^{\alpha}_{0}+\frac{\gamma^{2}}{2}\left(\sum_{\alpha}\boldsymbol{s}^{\alpha}_{0}\otimes\boldsymbol{m}^{\alpha}_{0}\right)^{2}+\frac{\gamma^{3}}{6}\left(\sum_{\alpha}\boldsymbol{s}^{\alpha}_{0}\otimes\boldsymbol{m}^{\alpha}_{0}\right)^{3}, \tag{3.21}$$

with cumulative slip γ to be determined in the analysis. This slip may result from dislocation glide, deformation twinning, and/or sliding of micro-cracks. For uniaxial strain compression, mode I crack opening is omitted, and inelasticity is isochoric ($\boldsymbol{s}^{\alpha}_{0}\cdot\boldsymbol{m}^{\alpha}_{0}=0\ \Rightarrow\ J^{\mathrm{P}}=1$). From geometry of the problem, all n systems experience the same resolved shear stress $\tau=\tau^{\alpha}$. Normalizing (3.14) by shear modulus (2.82) or (2.83), the prescribed yield criterion in the plastically deforming regime is

$$\tau/\mathsf{G}_{0}=g(\xi)/\mathsf{G}_{0}=g_{0}-\chi\xi;\quad \xi=n\gamma. \tag{3.22}$$

Here, g_0 is dimensionless initial shear strength at the HEL, dependence of strength $g=g^{\alpha}$ on temperature is omitted, and internal state variable ξ is the total slip on all n systems. Material constant $\chi\geqslant 0$ accounts for loss of shear resistance as fracture ensues in conjunction with dislocation slip or twinning. For the brittle solids considered here, such strength loss far exceeds any hardening that might arise from dislocation accumulation. In $U=U^{-}$ of (3.15), it is assumed $\kappa=0$ since prior analysis (Clayton, 2009, 2010a, 2010c, 2011b) confirms that stored energy of lattice defects should be negligible relative to plastic dissipation in strong ceramics under uniaxial compression, insignificantly affecting the predicted thermomechanical response.

Crystalline quartz is known to have a large number of possible cleavage planes with very similar surface energy, and is also prone to conchoidal fracture (Schultz, Jensen, & Bradt, 1994), i.e., curved failure surfaces not confined to any particular plane, as observed in glass. Dislocation slip (Clayton, Chung, Grinfeld, & Nothwang, 2008) and Dauphné twinning (Barton & Wenk, 2009) which may occur at high temperatures are omitted in the present description of quartz under shock compression. Therefore, inelastic deformation consisting of modeII/III cracks on numerous, possibly curved surfaces in quartz is modeled as isochoric and isotropic:

$$\boldsymbol{F}^{\mathrm{P}}(\gamma)=\begin{bmatrix} 1-\gamma & 0 & 0\\ 0 & (1-\gamma)^{-1/2} & 0\\ 0 & 0 & (1-\gamma)^{-1/2}\end{bmatrix}. \tag{3.23}$$

Yield criterion (3.22) applies with $n=1$ and maximum shear stress $\tau=J|\sigma_1-\sigma_3|$ used in place of τ^{α}, where $(\sigma_1,\sigma_2,\sigma_3)$ are principal Cauchy stress components.

Assume that HEL shock stress P_{H} is known from experimental data. Then the upstream (HEL) state is fully determined by the solution in Section 2.2, specifically (2.73)–(2.76) and (2.77). Specifically, $e=\ln J=\ln F$ is decreased incrementally until (2.74) reaches P_{H}, at which point $F=F^{+}$ and $U=U^{+}$. Given total deformation F^{-} and slip variable γ, thermoelastic deformation in behind the plastic shock is known from $\boldsymbol{F}^{\mathrm{E}}=\boldsymbol{F}(F^{-})\boldsymbol{F}^{\mathrm{P}-1}(\gamma)$. Internal energy, axial shock stress, and shear stress can then be written in the form

$$U^{-}=U^{-}(F^{-},\gamma,\eta^{-}),\quad P^{-}=P^{-}(F^{-},\gamma,\eta^{-}),\quad \tau=\tau(F^{-},\gamma,\eta^{-}). \tag{3.24}$$

Let $F^{-}=(\frac{V}{V_0})^{-}$ be prescribed as the load parameter. Then energy balance (3.19) and yield criterion (3.22) comprise two coupled algebraic equations that can be solved simultaneously for γ and η^{-}:

$$U^{-}(F^{-},\gamma,\eta^{-})-U^{+}=\frac{1}{2}[P^{-}(F^{-},\gamma,\eta^{-})+P_{\mathrm{H}}][F^{+}-F^{-}], \tag{3.25}$$

$$\tau(F^{-},\gamma,\eta^{-})/\mathsf{G}_{0}=g_{0}-n\gamma. \tag{3.26}$$

To obtain Hugoniot stress versus volume curves reported later in Section 3.3, (3.26) and (3.25) are solved simultaneously for γ and η^- as F^- is decreased incrementally below $\frac{V}{V_0}$ from the HEL state. With shock stress computed from the second of (3.24), plastic shock velocity $\mathfrak{D}$ and downstream particle velocity v^- can be obtained from the Hugoniot equations for mass and momentum conservation, (3.16) and (3.17), leading to (Molinari & Ravichandran, 2004)

$$\mathfrak{D} = \{(P^- - P_H)/[\rho_0(F^+ - F^-)]\}^{1/2}, \quad v^- = v^+ - \mathfrak{D}(F^- - F^+). \tag{3.27}$$

The downstream state is now fully known. The above procedure signifies the first known (reported) analytical solution for shock compression of anisotropic nonlinear thermoelastic–plastic single crystals, albeit restricted to planar shocks in highly symmetric crystal orientations. Previous analytical solutions have been restricted to linear isentropic elasticity (Johnson, 1972; Johnson, 1974; Johnson et al., 1970) in anisotropic crystals or to finite strain isotropic elastoplasticity (Perrin & Delannoy-Coutris, 1983).

3.3. Results: elastic–plastic solution

Elastic–plastic solutions of Section 3.2 are now applied to three single crystals: Z-cut sapphire, X-cut diamond, and X- and Z-cut quartz. Inelastic deformation mechanisms contributing to cumulative shear γ and inelastic properties n, g_0, and χ (respectively the number of shear systems, initial dimensionless shear strength, and rate of strength reduction with cumulative inelastic shear) are listed in Table 3. Also shown is the predicted value of cumulative shear γ_F at which the Hugoniot stress approaches the hydrostatic pressure–volume curve of (A.2) given in the Appendix A ($P \to p$ as $\gamma \to \gamma_F$). Particular entries of Table 3 are discussed in detail for each material in conjunction with predicted Hugoniot stress-volume curves in what follows next.

For Z-cut sapphire, preferred deformation mechanisms are rhombohedral (R-plane) twinning and R-plane fracture, which occur equally on three $\{\bar{1}012\}\langle\bar{1}01\bar{1}\rangle$ shear systems ($n = 3$). Previous analysis and experiments have confirmed that R-plane twinning is preferred over all other glide and twinning mechanisms for this orientation (Clayton, 2009; Fuller, Winey, & Gupta, 2013). Fracture is also most likely to occur on these planes, which have relatively low surface energy (Schultz et al., 1994); dynamic R-plane cleavage has been confirmed by high speed photography in impact experiments (McCauley, Strassburger, Patel, Paliwal, & Ramesh, 2013). Initial yield strength for twinning at the HEL is predicted as $g \approx 0.044 G_0 = 7.3$ GPa, near the upper bound of ranges $1 \lesssim g \lesssim 8$ GPa quoted for R-twinning from previous analyses of indentation (Tymiak & Gerberich, 2007) and uniaxial strain (Clayton, 2009). Noting that the characteristic twinning shear for this twin system is $\gamma_T = 0.202$ (Clayton, 2009), the maximum volume fraction of twinned material for each system is $\frac{\gamma_E}{\gamma_T} \approx 0.3$. Predicted Hugoniot stress is compared with experimental data (Graham & Brooks, 1971) in Fig. 4. The HEL

Table 3
Inelastic deformation mechanisms and properties for single crystals.

Material	Orientation	Mechanism(s)	n	g_0	χ	γ_F
Sapphire	Z	$\{\bar{1}012\}\langle\bar{1}01\bar{1}\rangle$ twinning and cleavage	3	0.044	0.25	0.06
Diamond	X	$\{111\}\langle\bar{1}10\rangle$ glide and cleavage	8	0.041	0.10	0.04
	X	$\{111\}\langle\bar{2}11\rangle$ glide and cleavage	4	0.047	0.10	0.07
Quartz	X	conchoidal fracture	1	0.047	0.33	0.10
	Z	conchoidal fracture	1	0.087	0.50	–

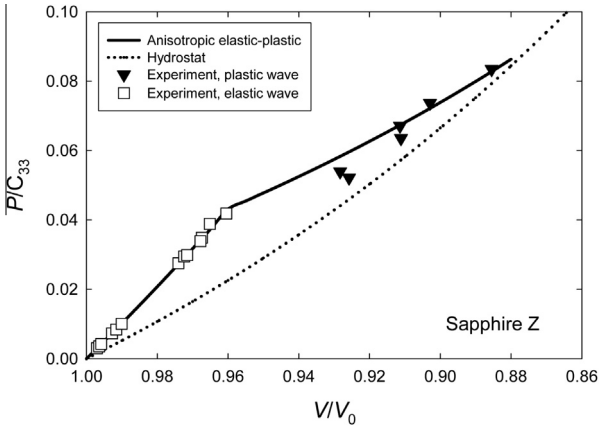

Fig. 4. Nonlinear elastic–plastic solution and experimental data (Graham & Brooks, 1971) for Z-cut sapphire: shock stress vs. volume ratio.

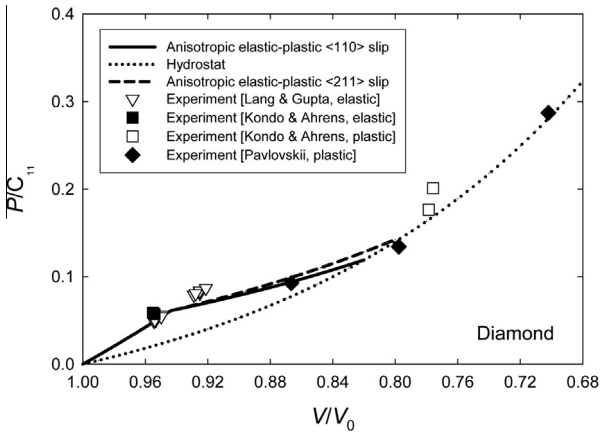

Fig. 5. Nonlinear elastic–plastic solutions and experimental data (Lang & Gupta, 2010; Kondo & Ahrens, 1983; Pavlovskii, 1971) for diamond: shock stress vs. volume ratio.

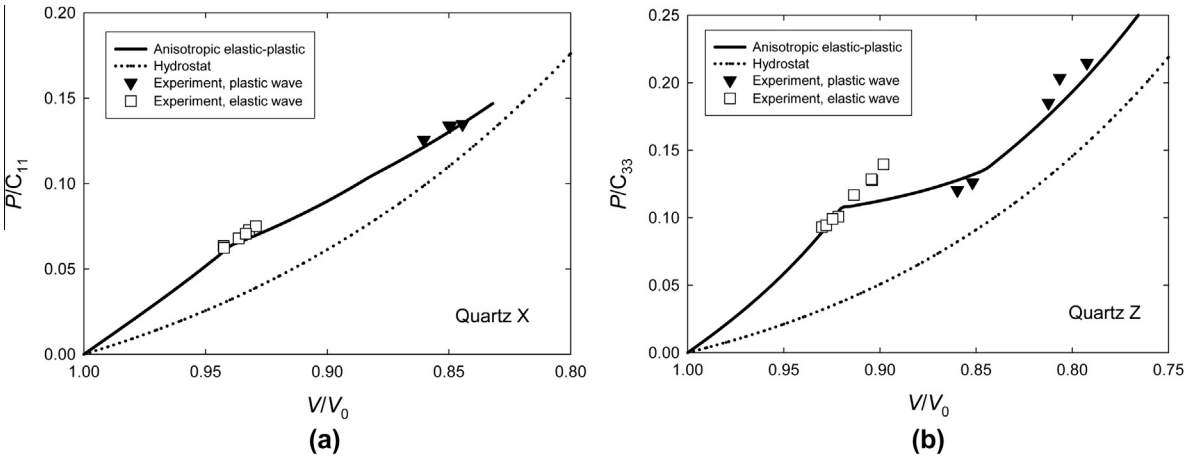

Fig. 6. Nonlinear elastic–plastic solutions and experimental data (Fowles, 1967) for quartz: (a) shock stress vs. volume ratio, X-cut (b) shock stress vs. volume ratio, Z-cut.

corresponds to $\frac{V}{V_0} \approx 0.96$, at which point twinning initiates according to the model. In the plastic regime, Hugoniot stress collapses to the hydrostat of (A.2) for $\frac{V}{V_0} \lesssim 0.88$. Since strength decreases ($\chi > 0$), fracture on R-planes accompanies twinning.

For X-cut diamond, two possible preferred deformation mechanisms are considered separately: (i) octahedral slip and octahedral plane fracture which occur equally on eight $\{1\,1\,1\}\langle\bar{1}\,1\,0\rangle$ shear systems ($n = 8$) and (ii) slip and octahedral plane fracture which occur equally on four $\{1\,1\,1\}\langle\bar{2}\,1\,1\rangle$ shear systems ($n = 4$). These two sets of systems have been suggested elsewhere (Lang & Gupta, 2010 and references therein) for diamond, the first being reported more often. Fracture is most likely to occur on $\{1\,1\,1\}$ planes, which have low surface energy (Schultz et al., 1994) and low cleavage strength predicted from first principles (Telling, Pickard, Payne, & Field, 2000). Initial yield strength for slip at the HEL is predicted as $g \approx 0.041 G_0 = 22$ GPa for $\langle\bar{1}\,1\,0\rangle$ systems and $g \approx 0.047 G_0 = 25$ GPa for $\langle\bar{2}\,1\,1\rangle$ systems. These predictions are within ranges $19 \lesssim g \lesssim 30$ GPa for $\langle\bar{1}\,1\,0\rangle$ and $23 \lesssim g \lesssim 35$ GPa for $\langle\bar{2}\,1\,1\rangle$ estimated in Lang and Gupta (2010) using isentropic Lagrangian elasticity. Using isotropic elasticity, a shear strength of 30 GPa has also been estimated from shock data (Kondo & Ahrens, 1983). Predicted Hugoniot stress is compared with experimental data (Kondo & Ahrens, 1983; Lang & Gupta, 2010; Pavlovskii, 1971) in Fig. 5. While shock experiments were along [100] directions in Lang and Gupta (2010), Kondo and Ahrens (1983), and Pavlovskii (1971), shock experiments in Kondo and Ahrens (1983) were not along pure mode directions, so model predictions are only approximately representative of the latter data. In the model, the representative HEL corresponds to $\frac{V}{V_0} \approx 0.94$, towards the upper end of the range of values reported in Lang and Gupta (2010) and consistent with experiments of Kondo and Ahrens (1983). In the plastic regime, Hugoniot stress collapses to the hydrostat of (A.2) for $\frac{V}{V_0} \lesssim 0.82$ for $\langle\bar{1}\,1\,0\rangle$ systems or $\frac{V}{V_0} \lesssim 0.80$ for $\langle\bar{2}\,1\,1\rangle$ systems. Strength decreases at the same rate ($\chi = 0.10$) for each model prediction, meaning fracture on octahedral planes accompanies dislocation glide in each case. While both sets of slip systems enable accurate representation of experimental data, the present calculations suggest that $\{1\,1\,1\}\langle\bar{1}\,1\,0\rangle$ slip should be more likely to occur

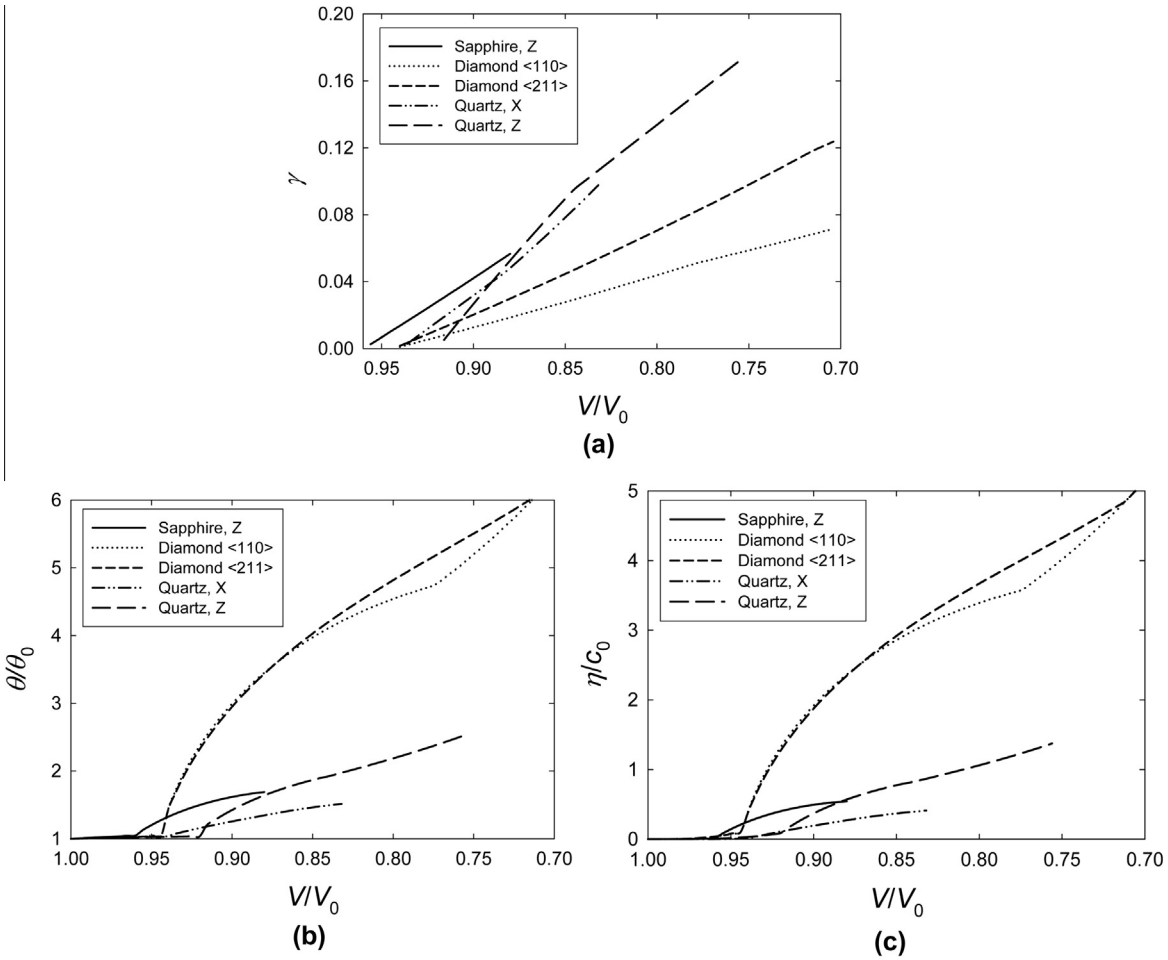

Fig. 7. Nonlinear elastic–plastic solutions: (a) cumulative slip or inelastic shear (b) temperature (c) entropy.

than $\{1\,1\,1\}\langle\bar{2}\,1\,1\rangle$ slip since g_0 is lower in the former. More slip accumulates on each individual system in the latter set (i.e., larger γ_F in Table 3 for $\langle\bar{2}\,1\,1\rangle$) since there are fewer systems ($n = 4$) for this set.

For X- and Z-cut quartz, conchoidal fracture or simultaneous cleavage of a large number of planes (Schultz et al., 1994) is modeled using the isotropic representation of inelastic deformation in (3.23). Yield is permitted to be anisotropic through prescription of different values of g_0 and χ depending on orientation. This approach enables successful fitting to Hugoniot data (Fowles, 1967) in Fig. 6, but is not fully predictive since experimental data are insufficient to parameterize shear strength for arbitrary crystal orientations. Initial yield strength for fracture at the HEL is computed as $g \approx 0.047G_0 = 2.3$ GPa for X-cut quartz and $g \approx 0.087G_0 = 4.2$ GPa for Z-cut. In the model, the representative HEL corresponds to $\frac{V}{V_0} \approx 0.94$ for X-cut and $\frac{V}{V_0} \approx 0.92$ for Z-cut. In the plastic regime, Hugoniot stress nears the hydrostat of (A.2) for $\frac{V}{V_0} \lesssim 0.84$ for X-cut quartz in Fig. 6(a), wherein $\gamma \approx \gamma_F = 0.1$. In Fig. 6(b), data from Fowles (1967) remain above the logarithmic hydrostat to volumetric compression in excess of 20%. For this reason, no value of γ_F is listed for Z-cut quartz in Table 3, and $\chi \to 0$ for $\gamma > 0.092$ is imposed in calculations for this orientation.

Theoretical predictions of cumulative slip, temperature, and entropy are shown for all crystal types in respective Fig. 7(a)–(c). All three variables are closely related since entropy and temperature increase in conjunction with energy dissipated by inelastic deformation in the plastic regime. Temperature rise and entropy production are comparatively small in the elastic regime [Fig. 7(b) and (c)] as noted already in Section 2.3 and Table 2. Predicted temperature rise and normalized entropy production are largest for diamond because it has by far the largest absolute shear strength g and the smallest c_0 (Table 1) of the three crystals.

4. Conclusions

Finite strain thermoelastic and thermoelastic–plastic constitutive theories incorporating a logarithmic elastic strain measure referred to material coordinates have been developed for anisotropic single crystals and applied towards shock

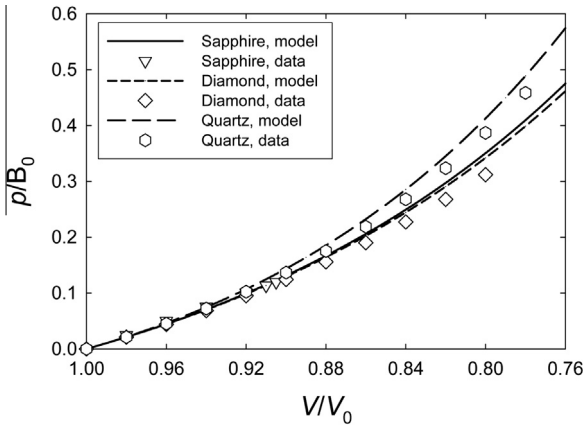

Fig. 8. Logarithmic EOS predictions and experimental data (Hart & Drickamer, 1965; Occelli et al., 2003; Kimizuka et al., 2007) for hydrostatic compression of sapphire, diamond, and quartz.

compression problems. New analytical solutions have been derived for planar elastic and plastic shocks along directions of high symmetry. Predictions have been analyzed for sapphire, diamond, and quartz single crystals. In the elastic regime, superior accuracy of the proposed logarithmic theory over existing Lagrangian and Eulerian theories has been demonstrated for sapphire, diamond, and Z-cut quartz. In the plastic regime, constitutive relations and necessary parameters have been developed and determined that describe experimental Hugoniot data, including the loss of shear strength for sapphire, diamond, and X-cut quartz observed at shock stresses exceeding the HEL and the corresponding collapse of the Hugoniot stress to the hydrostat. Accuracy of the latter described by a logarithmic pressure–volume EOS has been demonstrated. Precise values of rhombohedral twinning resistance in sapphire and octahedral slip resistance in diamond have been calculated; these compare favorably with coarse estimates given elsewhere. Model results for quartz suggest that fracture criteria are highly orientation dependent despite the availability of numerous low-energy planes for potential cleavage and experimental evidence of conchoidal fracture.

Appendix A. Hydrostatic compression

Considered here is the pressure–volume equation-of-state (EOS) derived from the logarithmic nonlinear elasticity theory of Sections 2.1 and 3.1. Assume adiabatic conditions, isochoric plastic deformation (if any) such that $J = \det \boldsymbol{F} = J^{\mathrm{E}}$ consists only of thermoelastic volume change, and a hydrostatic stress state such that $\boldsymbol{\sigma} = -p\mathbf{1}$, with p the Cauchy pressure. Then balance of energy (2.7) degenerates to

$$\dot{U} = J\boldsymbol{\sigma} : \nabla \boldsymbol{v} = -Jp\nabla \cdot \boldsymbol{v} = -p\dot{J}. \tag{A.1}$$

For materials with less than cubic symmetry, deviatoric components of deformation rate may be nonzero, but only volume changes contribute to internal energy. Pressure obeys, for logarithmic nonlinear elasticity, the following EOS (Poirier & Tarantola, 1998):

$$p = -(\partial \check{U}/\partial J)|_{\Delta\eta=0} = -\mathrm{B}_0[(\ln J)/J]\left[1 - \frac{1}{2}(\mathrm{B}_0' - 2)\ln J\right], \tag{A.2}$$

where B_0 is the isentropic bulk modulus and B_0' the pressure derivative of the bulk modulus in the unstressed reference state. For isothermal hydrostatic loading, free energy and isothermal constants replace internal energy and isentropic constants in (A.2). For $2 \leqslant \mathrm{B}_0' \leqslant 5$ and $\frac{2}{3} \leqslant J \leqslant 1$, differences in pressure predicted by logarithmic EOS (A.2) and the second-order Birch–Murnaghan (B–M) EOS associated with Eulerian elasticity (Clayton, 2013; Jeanloz, 1989) are insignificant, but at very high compression – as occurring in the Earth's interior for example – the logarithmic EOS becomes more realistic than the B–M EOS (Poirier & Tarantola, 1998).

Predictions of (A.2) are compared with experimental hydrostatic compression data on sapphire (Hart & Drickamer, 1965), diamond (Occelli, Loubeyre, & LeToullec, 2003), and quartz (Kimizuka, Ogata, Li, & Shibutani, 2007) in Fig. 8. Pressures are limited to those under which phase transformations might occur. Close agreement with all data is evident for $\frac{V}{V_0} \gtrsim 0.88$. Predictions are made using isentropic bulk moduli from (2.80) or (2.81) and pressure derivatives obtained from ultrasonic data (Gieske & Barsch, 1968; McSkimin & Andreatch, 1972; McSkimin et al., 1965), all listed in Table 1, i.e., the EOS parameters were obtained independently and are not fit directly to the high pressure data shown. The EOS predictions tend to exceed the data for diamond and quartz for $\frac{V}{V_0} \lesssim 0.88$; the discrepancy is due in part to use of isentropic elastic constants (more appropriate for comparison with shock data in Section 3.3) rather than isothermal constants.

References

Anand, L. (1979). On H. Hencky's approximate strain-energy function for moderate deformations. *Journal of Applied Mechanics, 46*, 78–82.

Aslan, O., Cordero, N., Gaubert, A., & Forest, S. (2011). Micromorphic approach to single crystal plasticity and damage. *International Journal of Engineering Science, 49*, 1311–1325.

Bammann, D. (1984). An internal variable model of viscoplasticity. *International Journal of Engineering Science, 22*, 1041–1053.

Barton, N., & Wenk, H.-R. (2009). Dauphiné twinning in polycrystalline quartz. *Modelling and Simulation in Materials Science and Engineering, 15*, 369–384.

Barton, N., Winter, N., & Reaugh, J. (2009). Defect evolution and pore collapse in crystalline energetic materials. *Modelling and Simulation in Materials Science and Engineering, 17*, 035003.

Clayton, J. (2005a). Dynamic plasticity and fracture in high density polycrystals: Constitutive modeling and numerical simulation. *Journal of the Mechanics and Physics of Solids, 53*, 261–301.

Clayton, J. (2005b). Modeling dynamic plasticity and spall fracture in high density polycrystalline alloys. *International Journal of Solids and Structures, 42*, 4613–4640.

Clayton, J. (2006). Continuum multiscale modeling of finite deformation plasticity and anisotropic damage in polycrystals. *Theoretical and Applied Fracture Mechanics, 45*, 163–185.

Clayton, J. (2008). A model for deformation and fragmentation in crushable brittle solids. *International Journal of Impact Engineering, 35*, 269–289.

Clayton, J. (2009). A continuum description of nonlinear elasticity, slip and twinning, with application to sapphire. *Proceedings of the Royal Society of London Series A, 465*, 307–334.

Clayton, J. (2010a). Modeling nonlinear electromechanical behavior of shocked silicon carbide. *Journal of Applied Physics, 107*, 013520.

Clayton, J. (2010b). Deformation, fracture, and fragmentation in brittle geologic solids. *International Journal of Fracture, 163*, 151–172.

Clayton, J. (2010c). Modeling finite deformations in trigonal ceramic crystals with lattice defects. *International Journal of Plasticity, 26*, 1357–1386.

Clayton, J. (2011a). *Nonlinear mechanics of crystals*. Dordrecht: Springer.

Clayton, J. (2011b). A nonlinear thermomechanical model of spinel ceramics applied to aluminum oxynitride (AlON). *Journal of Applied Mechanics, 78*, 011013.

Clayton, J. (2012). On anholonomic deformation, geometry, and differentiation. *Mathematics and Mechanics of Solids, 17*, 702–735.

Clayton, J. (2013). Nonlinear Eulerian thermoelasticity for anisotropic crystals. *Journal of the Mechanics and Physics of Solids, 61*, 1983–2014.

Clayton, J., & Becker, R. (2012). Elastic–plastic behavior of cyclotrimethylene trinitramine single crystals under spherical indentation: Modeling and simulation. *Journal of Applied Physics, 111*, 063512.

Clayton, J., & Bliss, K. (2014). Analysis of intrinsic stability criteria for isotropic third-order green elastic and compressible neo-hookean solids. *Mechanics of Materials, 68*, 104–119.

Clayton, J., Chung, P., Grinfeld, M., & Nothwang, W. (2008). Kinematics, electromechanics, and kinetics of dielectric and piezoelectric crystals with lattice defects. *International Journal of Engineering Science, 46*, 10–30.

Clayton, J. (in press). Defects in nonlinear elastic crystals: Differential geometry, finite kinematics, and second-order analytical solutions. Zeitschrift für Angewandte Mathematik und Mechanik (ZAMM). doi: 10.1002/zamm.201300142.

Clayton, J., McDowell, D., & Bammann, D. (2004). A multiscale gradient theory for single crystalline elastoviscoplasticity. *International Journal of Engineering Science, 42*, 427–457.

Dluż ewski, P. (2000). Anisotropic hyperelasticity based on general strain measures. *Journal of Elasticity, 60*, 119–129.

Foulk, J., & Vogler, T. (2010). A grain-scale study of spall in brittle materials. *International Journal of Fracture, 163*, 225–242.

Fowles, R. (1967). Dynamic compression of quartz. *Journal of Geophysical Research, 72*, 5729–5742.

Fuller, H., Winey, J., & Gupta, Y. (2013). Inelastic deformation in shocked sapphire single crystals. *Journal of Applied Physics, 113*, 226102.

Germain, P., & Lee, E. (1973). On shock waves in elastic–plastic solids. *Journal of the Mechanics and Physics of Solids, 21*, 359–382.

Gieske, J., & Barsch, G. (1968). Pressure dependence of the elastic constants of single crystalline aluminum oxide. *Physica Status Solidi B Basic Solid State Physics, 29*, 121–131.

Grady, D. (1984). Microstructural effects on wave propagation in solids. *International Journal of Engineering Science, 22*, 1181–1186.

Graham, R. (1972). Determination of third- and fourth-order longitudinal elastic constants by shock compression techniques–application to sapphire and fused quartz. *Journal of the Acoustical Society of America, 51*, 1576–1581.

Graham, R., & Brooks, W. (1971). Shock-wave compression of sapphire from 15 to 420 kbar. The effects of large anisotropic compressions. *Journal of Physics and Chemistry of Solids, 32*, 2311–2330.

Guinan, M., & Steinberg, D. (1974). Pressure and temperature derivatives of the isotropic polycrystalline shear modulus for 65 elements. *Journal of Physics and Chemistry of Solids, 35*, 1501–1512.

Hankey, R., & Schuele, D. (1970). Third-order elastic constants of Al_2O_3. *Journal of the Acoustical Society of America, 48*, 190–202.

Hart, H., & Drickamer, H. (1965). Effect of high pressure on the lattice parameters of Al_2O_3. *Journal of Chemical Physics, 43*, 2265–2266.

Jeanloz, R. (1989). Shock wave equation of state and finite strain theory. *Journal of Geophysical Research, 94*, 5873–5886.

Jog, C. (2008). The explicit determination of the logarithm of a tensor and its derivative. *Journal of Elasticity, 93*, 141–148.

Johnson, J. (1972). Calculation of plane-wave propagation in anisotropic elastic–plastic solids. *Journal of Applied Physics, 43*, 2074–2082.

Johnson, J. (1974). Wave velocities in shock-compressed cubic and hexagonal single crystals above the elastic limit. *Journal of Physics and Chemistry of Solids, 35*, 609–616.

Johnson, J., Jones, O., & Michaels, T. (1970). Dislocation dynamics and single-crystal constitutive relations: Shock-wave propagation and precursor decay. *Journal of Applied Physics, 41*, 2330–2339.

Kimizuka, H., Ogata, S., Li, J., & Shibutani, Y. (2007). Complete set of elastic constants of α-quartz at high pressure: A first-principles study. *Physical Review B, 75*, 054109.

Kondo, K., & Ahrens, T. (1983). Shock compression of diamond crystal. *Geophysical Research Letters, 10*, 281–284.

Lang, J., & Gupta, Y. (2010). Strength and elastic deformation of natural and synthetic diamond crystals shock compressed along [100]. *Journal of Applied Physics, 107*, 113538.

Luscher, D., Bronkhorst, C., Alleman, C., & Addessio, F. (2013). A model for finite-deformation nonlinear thermomechanical response of single crystal copper under shock conditions. *Journal of the Mechanics and Physics of Solids*, 1877–1894.

McCauley, J., Strassburger, E., Patel, P., Paliwal, B., & Ramesh, K. (2013). Experimental observations on dynamic response of selected transparent armor materials. *Experimental Mechanics, 53*, 3–29.

McQueen, R., Marsh, S., Taylor, J., Fritz, J., & Carter, W. (1970). The equation of state of solids from shock wave studies. In R. Kinslow (Ed.), *High velocity impact phenomena* (pp. 293–417). New York: Academic Press.

McSkimin, H., & Andreatch, P. (1972). Elastic moduli of diamond as a function of pressure and temperature. *Journal of Applied Physics, 43*, 2944–2948.

McSkimin, H., Andreatch, P., & Glynn, P. (1972). The elastic stiffness moduli of diamond. *Journal of Applied Physics, 43*, 985–987.

McSkimin, H., Andreatch, P., & Thurston, R. (1965). Elastic moduli of quartz versus hydrostatic pressure at 25 °C and −195.8 °C. *Journal of Applied Physics, 36*, 1624–1632.

Molinari, A., & Ravichandran, G. (2004). Fundamental structure of steady plastic shock waves in metals. *Journal of Applied Physics, 95*, 1718–1732.

Nielsen, O. (1986). Optical phonons and elasticity of diamond at megabar stresses. *Physical Review B, 34*, 5808–5819.

Occelli, F., Loubeyre, P., & LeToullec, R. (2003). Properties of diamond under hydrostatic pressures up to 140 GPa. *Nature Materials, 2*, 151–154.

Pavlovskii, M. (1971). Shock compression of diamond. *Soviet Physics, Solid State, 13*, 1741–1742.

Perrin, G., & Delannoy-Coutris, M. (1983). Analysis of plane elastic–plastic shock-waves from the fourth-order anharmonic theory. *Mechanics of Materials, 2*, 139–153.
Poirier, J.-P., & Tarantola, A. (1998). A logarithmic equation of state. *Physics of the Earth and Planetary Interiors, 109*, 1–8.
Rajagopal, K., & Srinivasa, A. (1998). Mechanics of the inelastic behavior of materials. Part 1: Theoretical underpinnings. *International Journal of Plasticity, 14*, 945–967.
Regueiro, R., Bammann, D., Marin, E., & Garikipati, K. (2002). A nonlocal phenomenological anisotropic finite deformation plasticity model accounting for dislocation defects. *Journal of Engineering Materials and Technology, 124*, 380–387.
Schultz, R., Jensen, M., & Bradt, R. (1994). Single crystal cleavage of brittle materials. *International Journal of Fracture, 65*, 291–312.
Srinivasa, A. (2012). On the use of the upper triangular (or QR) decomposition for developing constitutive equations for Green-elastic materials. *International Journal of Engineering Science, 60*, 1–12.
Telling, R., Pickard, C., Payne, M., & Field, J. (2000). Theoretical strength and cleavage of diamond. *Physical Review Letters, 84*, 5160–5163.
Teodosiu, C., & Sidoroff, F. (1976). A theory of finite elastoviscoplasticity of single crystals. *International Journal of Engineering Science, 14*, 165–176.
Thomsen, L. (1972). The fourth-order anharmonic theory: Elasticity and stability. *Journal of Physics and Chemistry of Solids, 33*, 363–378.
Thurston, R. (1974). Waves in solids. In C. Truesdell (Ed.), *Handbuch der physik VIA/4* (pp. 109–308). Berlin: Springer-Verlag.
Thurston, R., McSkimin, H., & Andreatch, P. (1966). Third-order elastic coefficients of quartz. *Journal of Applied Physics, 37*, 267–275.
Tymiak, N., & Gerberich, W. (2007). Initial stages of contact-induced plasticity in sapphire. I. Surface traces of slip and twinning. *Philosophical Magazine, 87*(33), 5143–5168.
Vogler, T., & Clayton, J. (2008). Heterogeneous deformation and spall of an extruded tungsten alloy: Plate impact experiments and crystal plasticity modeling. *Journal of the Mechanics and Physics of Solids, 56*, 297–335.
Wackerle, J. (1962). Shock wave compression of quartz. *Journal of Applied Physics, 33*, 922–937.
Wallace, D. (1972). *Thermodynamics of crystals*. New York: Wiley.
Wallace, D. (1980). Flow process of weak shocks in solids. *Physical Review B, 22*, 1487–1494.
Winey, J., & Gupta, Y. (2004). Nonlinear anisotropic description for shocked single crystals: Thermoelastic response and pure mode wave propagation. *Journal of Applied Physics, 96*, 1993–1999.
Winey, J., & Gupta, Y. (2006). Nonlinear anisotropic description for the thermomechanical response of shocked single crystals: Inelastic deformation. *Journal of Applied Physics, 99*, 023510.
Winey, J., Gupta, Y., & Hare, D. (2001). *R*-axis sound speed and elastic properties of sapphire single crystals. *Journal of Applied Physics, 90*, 3109–3111.
Xiao, H., Bruhns, O., & Meyers, A. (2007). Thermodynamic laws and consistent Eulerian formulation of finite elastoplasticity with thermal effects. *Journal of the Mechanics and Physics of Solids, 55*, 338–365.

1 (PDF) DEFENSE TECHNICAL INFORMATION CTR DTIC OCA

2 (PDF) DIRECTOR US ARMY RESEARCH LAB RDRL CIO LL IMAL HRA MAIL & RECORDS MGMT

1 (PDF) GOVT PRINTG OFC A MALHOTRA

36 (PDF) DIR USARL
RDRL CIH C
J KNAP
RDRL WM
R DONEY
B FORCH
J MCCAULEY
RDRL WML B
I BATYREV
D TAYLOR
N WEINGARTEN
RDRL WML H
B SCHUSTER
RDRL WMM
J BEATTY
RDRL WMM B
G GAZONAS
D HOPKINS
B POWERS
C RANDOW
RDRL WMM E
J SWAB
RDRL WMM F
T SANO
M TSCHOPP
RDRL WMM G
J ANDZELM
RDRL WMP
S SCHOENFELD
RDRL WMP A
D POWELL
RDRL WMP B
C HOPPEL
S SATAPATHY
M SCHEIDLER
A SOKOLOW
T WEERISOORIYA
RDRL WMP C
R BECKER
S BILYK
T BJERKE
D CASEM
J CLAYTON
D DANDEKAR
M GREENFIELD
R LEAVY
J LLOYD
M RAFTENBERG
S SEGLETES
C WILLIAMS

INTENTIONALLY LEFT BLANK.